Doctoral Dissertation

博士論文

Galactic Chemical Evolution and Origin of Heavy Elements Synthesized Through r-process and νp-process

（r プロセスおよび νp プロセスで合成される元素の銀河化学進化とその起源）

A Dissertation Submitted for the Degree of Doctor of Philosophy
December 2022

令和４年１２月博士（理学）申請

Department of Astronomy, Graduate School of Science,
The University of Tokyo

東京大学大学院理学系研究科天文学専攻

Yuta Yamazaki

山﨑 雄太

In gratitude, I doth profess
To mine alma mater's fond caress
For 'twas in her halls, with great delight
That knowledge shone, so clear and bright

Through toil and tears, I labored on
Each task a challenge, but here do I stand
For with each step, I came to see
The wonder of the world, so brilliantly

Now as I leave, with fond adieu
And venture forth, with courage anew
I shall take with me, this proud belief
That learning is power, and brings relief

And in the new realm, far and wide
Where fortune beckons, and worlds collide
I shall strive to bring, to every deed
The wisdom of the ages, so pure and deep

Thus, I doth pledge, with all my heart
To honour my education's noble art
And in all my ways, with steadfast might
To carry forward, its radiant light.

Abstract

There are more than one hundred elements in the present universe, and hundreds of nuclides are known, including isotopes. However, only a few of the lightest elements, such as hydrogen and helium, existed in the early universe immediately after the Big Bang. In other words, hundreds of heavier nuclides have gradually been produced over the long history of the universe up to the present day. Studies of how the elements in the present universe were created originated in the seminal review paper on elemental synthesis in celestial bodies written by Burbidge, Burbidge, Fowler, and Hoyle (BBFH). Since the BBFH paper, detailed processes of elemental synthesis and their source objects have been studied in both nuclear physics and astronomy. Although much remains to be understood in detail, two major questions remain. Two major questions remain: the origin of elements produced by the rapid neutron capture process (r-process) and the origin of proton-rich isotopes of stable elements (p-nuclei). Our study was initiated to calculate how these elements have evolved in galaxies considering various models and to provide a baseline for future astronomical observations. In this thesis, we present our theoretical predictions through two galactic chemical evolution studies on the r-process and the νp-process.

The first study was a galactic chemical evolution calculation, which shows the time evolution of all isotopes for the elements produced through r-process. One very important observational feature is known about the r-process elements in galactic stars. Namely, that the stars of the galaxy share a characteristic elemental abundance pattern, called 'universality'. This fact has long been interpreted to mean that the r-process only occurs in a single astrophysical environment. Indeed, the results of nucleosynthesis calculations of r-processes show a variety of isotopic abundance patterns, depending on the astrophysical object and model. Hence, considering their combination seems, at first glance, to contradict the observations. However, an examination of several recent studies of nucleosynthesis calculations shows that, within the range of elements covered by 'universality', similar patterns are produced by any astrophysical event currently modelled. Therefore, it is necessary to discuss chemical evolution in the universe by considering all these astrophysical sites, rather than studying just one of the three most likely sources of the r-process elements: supernova(SN), neutron star merger (NSM) and collapsar. Since each of these three astronomical events originated from different progenitors, there is a large difference in when in the history of the galaxy they occurred. This is expected to lead to a significant evolution of the abundance ratios of r-process elements. For the first time, we have performed GCE calculations taking all three sources into account. By using the One-zone model, a wide parameter space is examined, and four key model cases are discussed in this thesis. The common result for each model is a time-evolving

isotopic abundance ratio that, as expected, satisfies the observational constraint on the elemental abundance pattern, the 'universality'. The strong odd-even effect produced by a high entropy environment in collapsars will be observed in metal poor stars. Isotope separation by astronomical observation is still a challenge, however, the ratio of the sum of the odd-isotopes to that of the even-isotopes can be measured.

The second study was a study of the evolution of proton-rich nuclei. The fraction of p-nuclei is typically <1% for each element. Most of them are created by the γ-process in SNe. However, some elements, such as molybdenum and ruthenium, have a large fraction of p-nuclei. Such a large fraction of p-nuclei could not be produced by SNe γ-process. Recent nucleosynthesis calculations suggest that a process involving neutrinos, called νp-process, produces a large amount of molybdenum and ruthenium. Including this another process for p-nuclei synthesis, supernova or hypernova (HN), a more explosive type of supernova, creates a large fraction of p-nuclei for some elements. HN is an ideal site for νp-process since its high energy condition is mostly due to neutrinos. In this thesis, we performed GCE calculations considering all the nucleosynthetic process of heavy elements; s-process, r-process, γ-process, and νp-process. The result shows that the amounts of the p-nuclei synthesised through the νp-process in HNe or SNe are sufficient to reproduce large p-nuclei fractions of molybdenum and ruthenium. The produced isotopic ratios of molybdenum, ruthenium, and palladium are also in great agreement with those observed in the solar system. Moreover, the elemental abundance of molybdenum is enhanced in the metal poor epoch by 0.5 dex, which is large enough to be observed.

Acknowledgements

The past five years have been an exciting journey towards completing my Ph.D. at the University of Tokyo by writing this thesis. I would like to express my sincere gratitude to everyone who has helped me to reach the final destination - the successful completion of this thesis.

First of all, I would like to thank Toshitaka Kajino, my supervisor from the University of Tokyo, for his constant enthusiasm and guidance. His perspicacity inspired me to seek the truth and his geniality provided me with a hospitable workplace. He remained patient and steadfast in their guidance despite my shortcomings as a student. Without their expert tutelage, I would not have been able to achieve my doctorate degree. Their mentorship and professional wisdom have been invaluable to me and will continue to guide me throughout my career.

Furthermore, I am very grateful to Fumitaka Nakamura, my supervisor on documents. His help is essential to my research opportunities.

My thanks also go to my colleagues. G. J. Mathews provided me with the essential code, the first project in my five years of Ph.D. studies. Without his great efforts in our research discussions, I would not be standing here now. Hirokazu Sasaki, a senior member of the Kajino Lab, performed theoretical calculations that were indispensable for my research. We also wrote papers together, and I learned a lot from him as a young researcher. I would also like to thank the COSNAP members in Japan, U.S., and China. I am grateful for our fruitful discussions and they make my days enjoyable and memorable.

I would like to express my gratitude to the reviewers. Their expert guidance and insightful feedback greatly improved the quality of this thesis. Without their rigorous scrutiny and invaluable insights, my thesis would not have been the same.

My friends were indispensable in my pursuit of a degree. Their company over meals, play, and conversation refreshed me through difficult times. They have given me new joys and perspectives that are vital for my future. I express my deepest gratitude to M.S., T.H., H.T., T.N., and M.T.

Finally I would like to express my deepest gratitude to the people dearest to me. To my beloved parents, I offer heartfelt gratitude for nurturing me with love, and for steadfastly supporting me through trying times, despite my youthful mistakes. Your tender care has helped shape the person I am today, and the values and wisdom you

have imparted will always guide me on life's journey. I would also like to pay tribute to my dear brother Syunki. As siblings we have a special bond and I am grateful for his presence in my life. His support and companionship have brought me much joy.

I would like to extend my gratitude to my dear, Shoko, who has been by my side for the past decade, accompanying me through every step of my whole student life. I am grateful for her steadfast presence in my life.

Yuta,

Contents

1 The Astronomical Observations and Theoretical Studies of r-process elements

In this chapter we summarize the previous studies of heavy elements, especially of r-process elements. We will first present previous observations on r-process elements and their interpretations, while also presenting the most important background of our work; the possibility of new interpretations. Secondly, since the results of r-process nucleosynthesis calculations for each candidate object are important, we present nucleosynthesis calculations for supernova explosions, NSMs, and collapsars, and their characteristics.

1.1 The r-process abundance pattern

1.1.1 The universality of r-process elemental abundance pattern

By astronomical spectroscopic study of stellar atmosphere in galactic stars, we can estimate the abundance ratio between two elements, for instance, [Fe/H] and [Mg/Fe].

We consider that the atmosphere of stars keeps a record of the chemical composition of interstellar gas at the star birth. This assumption can be violated by mixing of core and atmospheric material due to the convection inside the stars. However, when we are interested in elements heavier than Oxygen, this assumption is justified, especially for low mass stars, since CNO cycle or triple-α reaction is the final chain of nuclear burning in stars with less than 5 solar mass. Moreover, that is more valid for r-process elements. High neutron flux required for r-process can not be achieved in 'normal' stars. Thus, stellar atmosphere is considered to represent a perfect record

of the r-process abundance at the time the stars formed.

As mentioned in the introduction section (Section **??**), s-process is more accessible compared with r-process. Therefore, the solar r-process abundance pattern is evaluated by subtracting the s-process abundance pattern from the total. The situation is easier for metal poor stars. The progenitors of AGB stars are low- to intermediate-mass stars. Besides, s-process is a 'secondary' process which needs seed nuclei. Thus, s-process contribution to abundance of neutron capture elements can appear only in the late stage of the galaxy ([Fe/H]>-2). On the other hand, r-process is a 'primary' process which proceed from protons and does not need seed nuclei. Therefore, we can assume that the heavy elements in metal poor stars are synthesized by only r-process.

From astronomical spectroscopy, Sneden *et al.* (2008) [1] suggested that elemental abundance of r-process in galactic halo stars show the very similar pattern as the solar one (Figure 1). This feature is called 'universality.' The universality of r-process abundance pattern extends atomic number (Z) from 37 to 92. The abundance variation in this range is around only 0.2 dex. This fact that many galactic stars share a universal feature is believed to be a clue that one single type of astrophysical event dominates the production of the r-process elements.

However, recent observations have shown that variations in abundance exist in a wide range of elements. The universality is valid only in the range of Z from 60 to 75, with exceptions outside this range. Here, two types of r-process abundance pattern variations will be given.

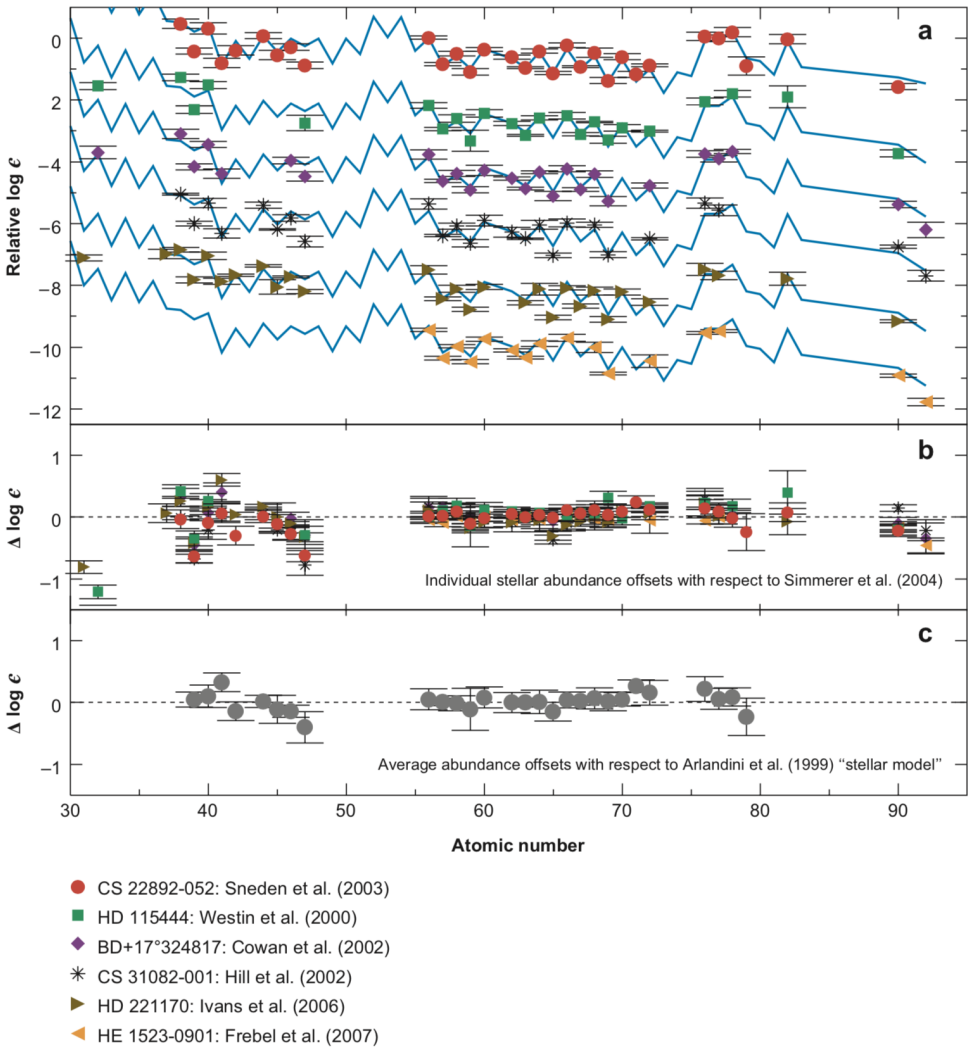

Fig. 1. Each colored dots shows the abundance pattern of galactic metal poor stars. Blue solid lines show the relative solar system abundance. Each abundance is added some constant value for visualizing purpose. The lower panel shows the discrepancy between low metal stars and solar system.
(reprinted from Sneden *et al.* 2008) [1]

1.1.2 Honda stars

Honda *et al.* (2006) [2] and Honda *et al.* (2007) [3] claimed the variation of elemental abundance pattern in light r-process elements (Figure 2). They analyzed the spectra of very metal poor stars (HD122563, HD88609 and etc.).

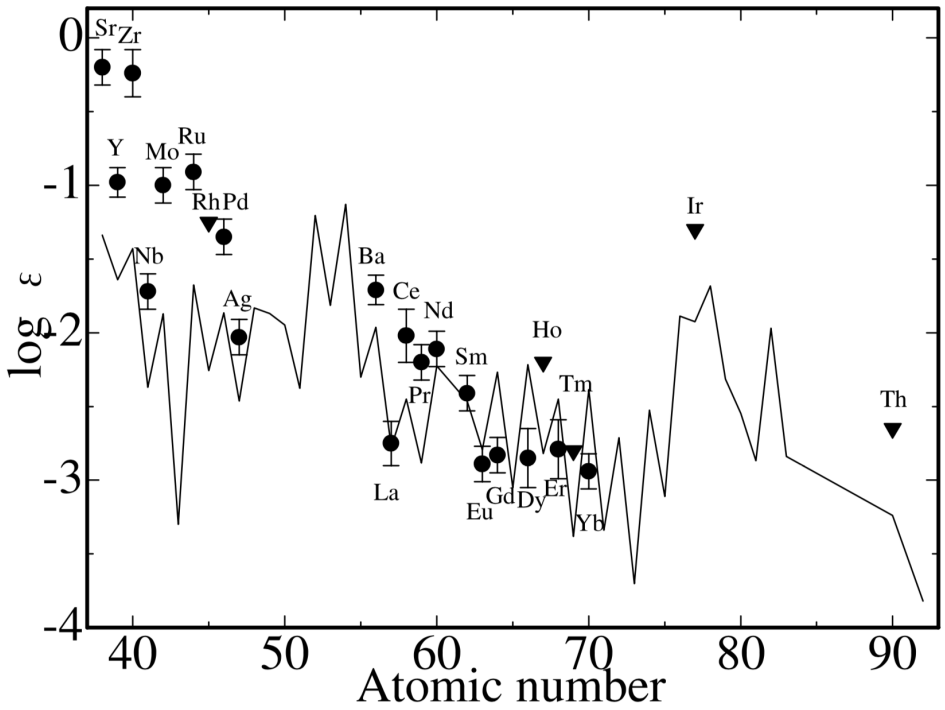

Fig. 2. Abundance of HD 88609. Dots show the observed abundance and solid line shows the relative solar abundance normalized at Europium.
(reprinted from Honda *et al.* 2007) [3]

They found that elements below the r-process second peak (Z<50) are clearly enhanced as shown in Figure 2. This enhanced abundance of light r-process elements might be explained by *weak r-process*. Also, the abundances of elements even around Z∼60 do not perfectly match to the solar system abundance. For a recent analysis, Aoki et al. (2017) reviewed the variation of light r-process elements [4]. They again confirmed that the r-process abundance in galactic stars strongly suggests multiple components of r-process source.

1.1.3 The maintained universality with multiple contributors

The observed elemental abundance patterns in many r-process enhanced metal-poor stars are very similar to the solar system abundance pattern (universality). The robustness of this universality is confirmed for the elements between the second and third abundance peaks, in particular for those having atomic numbers $55 \leq Z \leq 70$. However, Honda stars show departure from the universal abundance pattern, exhibiting relative enhancement in lighter mass range around the first peak. Similar but quantitatively different variation also is found in the heavier mass range of actinides. Such a dramatic enhancement of actinide abundances is observed in some galactic stars called actinide-boost stars (Mashonkina et al. 2014). Although there are such variations in wide mass range, the relative ratios of yields between two nuclei with adjacent mass numbers are strongly constrained by their nuclear properties. The important point is that although the universality is valid to a limited mass range, it should be satisfied even if many types of r-process sites contribute to the production of nuclei in this range. Therefore, the universality is a precious measure to identify the astrophysical sites and quantify the explosion conditions for a successful r-process as discussed by Shibagaki *et al.* (2016) [5] and also to be discussed in the Result section of this paper.

1.2 The abundance of r-process element as a function of metallicity

1.2.1 The observed abundance of magnesium and europium

In previous section 1.1, we focused on elemental abundances of certain stars and the patterns of them. In addition to this kind of analysis, we can discuss the time evolution of elemental abundance of galactic stars by plotting them into the [X/Fe]-[Fe/H] plane. The plot of [X/Fe] as a function of metallicity is very useful to see the trend of elemental evolution. Figure 3 shows the evolution of two representative elements.

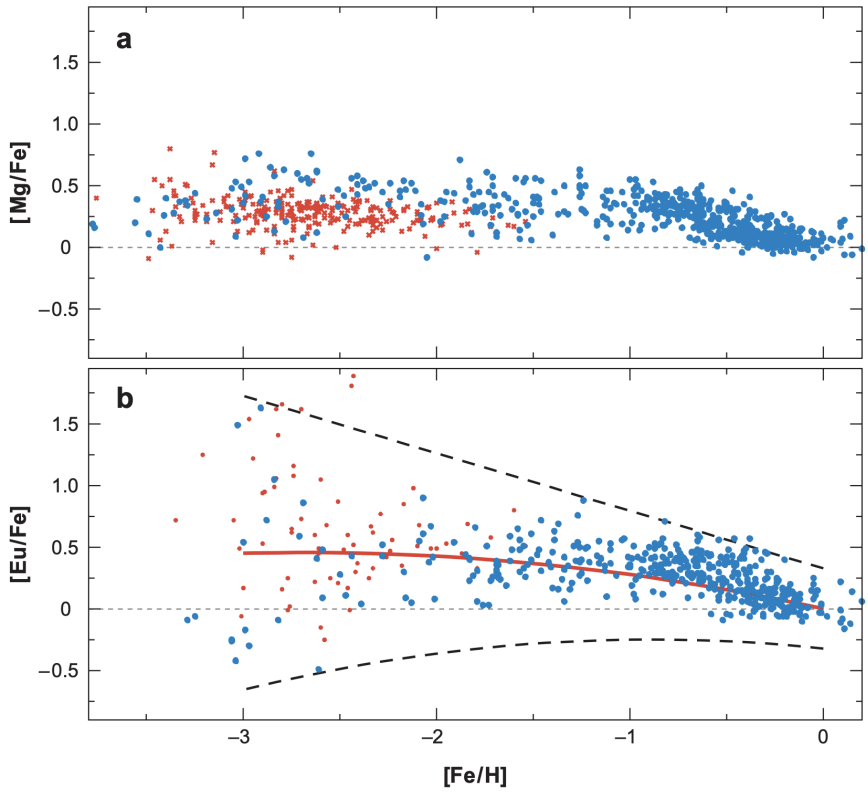

Fig. 3. [Mg/Fe] and [Eu/Fe] abundances as a function of [Fe/H] metallicity.
(reprinted from Sneden *et al.* 2008) [1]

Magnesium is mainly produced in massive stars which explode as CCSNe. In

metal poor era, Type Ia SN can not contribute to Iron abundance as mentioned in the previous section, therefore, CCSN is also the dominant source of Iron. Then, [Mg/Fe] becomes constant. After [Fe/H] reaches -1, Type Ia contribution appears and causes the descent of the ratio of Magnesium to Iron.

Europium is known as one of the most representative r-process elements since more than 95% of Europium in the universe is synthesized through r-process and much easier to detect by astronomical spectroscopy compared with other r-process elements. We can see the decreasing trend of [Eu/Fe] abundance, like Magnesium, at metal rich era ([Fe/H]>-1). In this sense, the galactic time dependency or r-process event rate have been considered to be 'CCSN-like.' At least, the enrichment rate of Europium is lower than that of Iron. On the other hand, in the metal poor era, we can see the difference from Magnesium. [Eu/Fe] abundance shows much larger scatter. This feature is considered as an effect of inhomogeneity of young galaxies or variation of r-process nucleosynthesis. Thus, the event rate of Europium production should be rarer than that of CCSN.

1.3 Nucleosynthesis Simulations

1.3.1 Neutrino Driven Wind (NDW)

The standard model of CCSN as a r-process site is neutrino driven wind(NDW). The iron core of a massive star collapse and numerous neutrinos are released at $\sim 10^{53}$ erg. These neutrinos drive the supernova explosion. The high neutron flux in this wind was considered to be ideal for r-process nucleosynthesis. However, recent calculations have found that electron fraction (or neutrons per seed ratio) is not enough to produce heavier r-process elements. Nevertheless, subsequent studies support that NDW can produce r-process nuclei up to $A \sim 130$. This process is so-called *weak r-process*. The produced abundance pattern up to $A \sim 125$ is very similar to that of the solar system. In this thesis, we used the $1.8M_{\odot}$ proto-neutron star model calculated by Wanajo (2013) [6]. The pattern is shown in Figure 4.

1.3.2 Magneto-hydro-dynamical Jet (MHDJ)

The standard model might be inadequate for a main r-process site. However, it was non-rotating and no magnetic fields model. Strong magnetic fields surrounding fast rotating proto-neutron stars enhance the explosion energy and the situation becomes favorable for the production of heavier r-process elements (A>130). Although such a strong magnetized neutron star much more rarely remains, neutron flux becomes so high in the magneto-hydrodynamically driven jets (MHDJ) from this kind of CCSNs. The fraction is estimated to be less than 1% in Winteler *et al.* (2012) [7]. It provides a rare r-process site in metal poor epoch required from the discussion on [Eu/Fe]-[Fe/H] plane mentioned in previous sections. In Figure 4, the produced abundance pattern for MHDJ is shown. It is taken from Nishimura *et al.* (2012) [8]. Many of the MHDJ nucleosynthesis simulations tend to produce a narrow r-process peak; just below and above the r-process peak in isotopic abundance pattern is underproduced. The model we used also have the same trend.

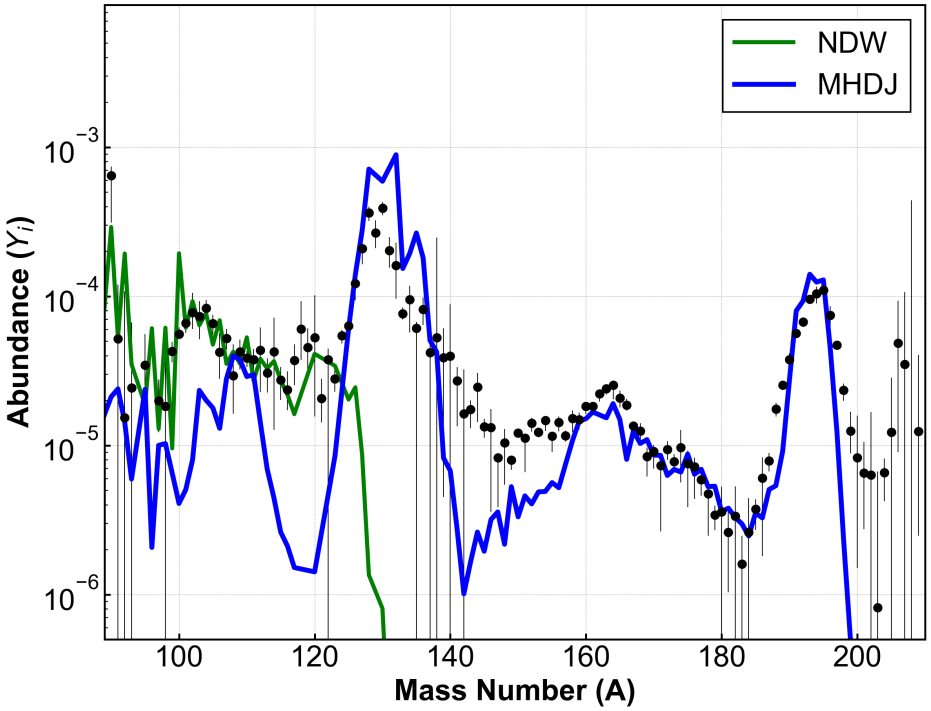

Fig. 4. Abundance pattern produced by NDW and MHDJ. Black dots shows the solar abundance. Green line shows abundance pattern by NDW normalized by A=115. Blue line shows abundance pattern by MHDJ normalized by A=175.

1.3.3 Neutron Star Merger (NSM)

Recently, binary neutron star merger is the most popular site for r-process. Since the detection of gravitational wave from a merging neutron star binary (GW170817) associated with a short duration gamma-ray burst (GRB170817a) and an astronomical transient called kilonova (AT2017gfo), many hydro-dynamical simulations and associated nucleosynthesis calculations have been done. Two types of ejecta are produced from one NSM event; dynamical-ejecta driven by tidal force of rotating binary and neutrino wind-ejecta driven by merging shock. Although the materials in both ejecta are very neutron rich, the physical condition is quite different. The condition of wind ejecta is very similar to NDW model. Wind ejecta, caused by the merging shock of binary neutron stars, is driven by neutrinos from merged neutron stars. Then, neutron flux is suppressed by n(ν, γ)p reaction that only *weak r-process* occurs. We used the abundance pattern calculated by Martin *et al.* [9]. On the other hand, dynamical-ejecta is formed by materials tidally blown off from neutron stars. In that region, electron fraction keeps so small ($Ye \sim 0.1$). Hence, r-process can proceed to the region of fissile nuclei (A$\sim$300). Fission fragment in this ejecta can capture neutrons again and then the process will repeat. This is so-called *fission recycling*. By repeated fission recycling, produced abundance pattern is dominated by fission fragment distribution. Fission fragment distribution is one of the unsolved problems in nuclear physics. We adopted abundance pattern from two nucleosynthesis calculation of dynamical-ejecta. One is calculated with symmetric fission fragment distribution and the other one is calculated with asymmetric fission distribution. Symmetric fission of massive nuclei around A$\sim$250-300 produce nuclei in A$\sim$120-150. This enhances the abundance just above the second peak. Contrary to this, asymmetric fission enhance the abundance of nuclei below or above the second peak. Then, the second peak is smoothed out. Suzuki *et al.* (2018) [10] and Shibagaki *et al.* (2016) [5] calculated the nucleosynthesis for the same dynamical-ejecta model but adopting different fission fragment distribution. (Former adopted symmetric one and latter used asymmetric one.) These three abundance patterns are shown in Figure 5

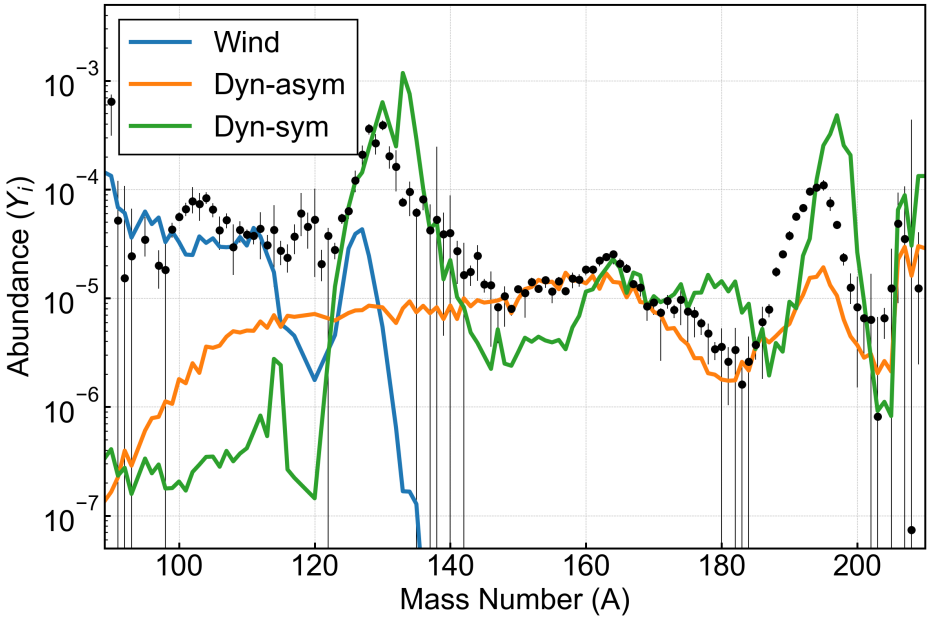

Fig. 5. Abundance pattern produced by dynamical-ejecta and wind-ejecta in NSM. Black dots shows the solar abundance. Blue line shows abundance pattern by wind-ejecta normalized by A=110. Orange line shows abundance pattern by dynamical ejecta calculated with symmetric fission fragment distribution (normalized by A=170). Green line shows abundance pattern by dynamical ejecta calculated with asymmetric fission fragment distribution (normalized by A=150).

As discussed here, the physical environments of dynamical-ejecta and wind-ejecta are totally different. However, the mass ratio between them is uncertain. Therefore, we assume two extreme cases in this study; dynamical-ejecta dominant model and wind-ejecta dominant model. The detailed model selection will be shown in section 2.

1.3.4 Collapsar

Another possible astrophysical site for r-process nucleosynthesis is the collapsar. When the core of massive star collapses into a black hole, an accretion disk is formed. The accretion disk is heated by neutrino-pair annihilation causing neutron rich matter to flow out from the disk into jets along the polar axis. This creates the conditions appropriate for r-process nucleosynthesis is provided. Most collapsar models involve relativistic jets which is observed as Long-duration Gamma Ray Burst (LGRB).

However, the physical condition of such a massive collapsing star has not been fully understood. The associated optical object depends on the astrophysical model of collapsars. In this paper, we, consider two types of numerical models. The first is the case of a failed-supernova. Nakamura *et al.* (2015) [11] proposed the collapsar as a promising candidate for a source of r-process elements. In this model, a massive progenitor collapses into a black hole without an energetic explosion, called failed-supernova. The entropy per baryon is so high that the r-process proceeds to an extremely neutron-rich region in the nuclear chart, then, produced abundance pattern, especially the second peak, is shifted to upper region as shown in Figure 6. And we can see the strong odd-even effect in the abundance pattern especially for $140<A<180$. In this study, we adopted the pattern calculated by Famiano et al. (2020), which is a follow-up study of Nakamura *et al.* (2015) [11]. The detailed characteristics of final yields will be discussed in section 3.1.2

The second model is the case that a collapsar is observed as a super-luminous supernova, or hypernova (HN). Siegel et al. (2019) ambitiously performed full GRMHD simulation of collapsar explosion. They claimed a sufficient amount of ^{56}Ni is produced by early shock heating of the star. The decay of huge amount of ^{56}Ni results in luminous optical emission and its luminosity reaches the value of a hypernova [12]. This model consists of three components of different physical condition ejecta. And the entropy per baryon is moderate compared with a previous model by Nakamura et al. (2015) or Famiano et al. (2020), therefore their final r-process yields show rather smooth and broad patterns (Figure 7).

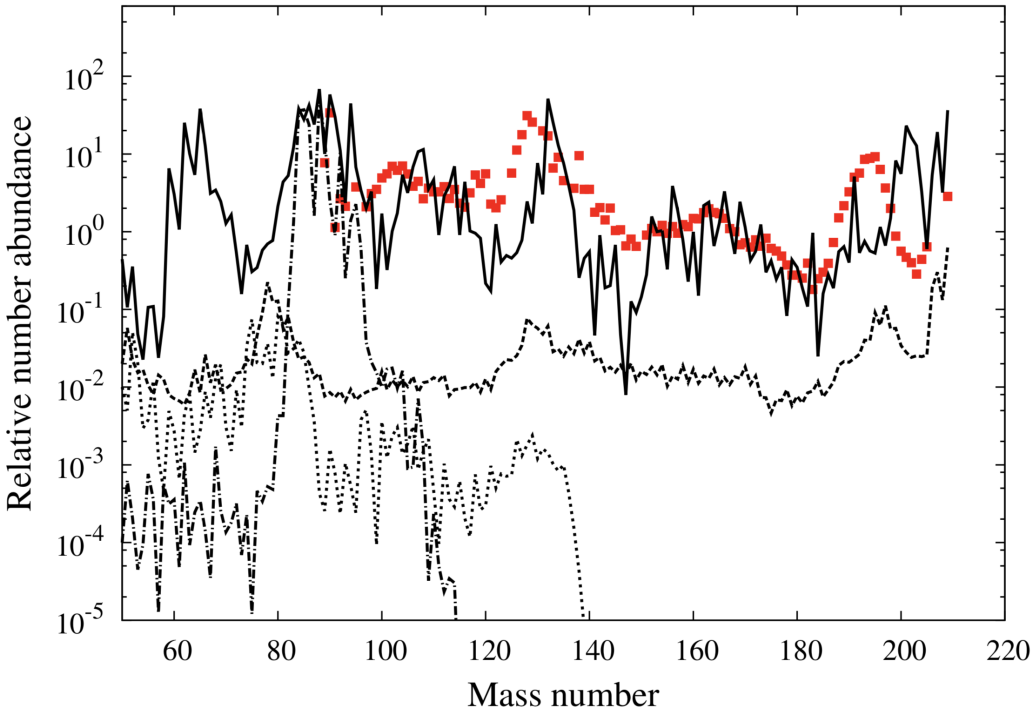

Fig. 6. The solid line shows the collapsar abundance pattern and red dot is solar abundance. (reprinted from Nakamura *et al.* 2015 [11])

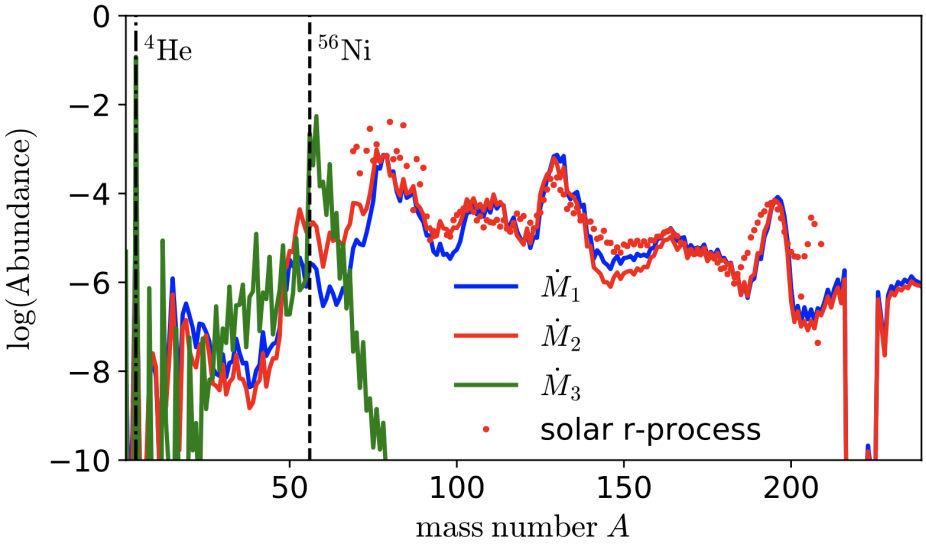

Fig. 7. Abundance patterns of synthesized r-process elements in the collapsar disk outflows at the three different accretion stages.
(reprinted from Fig.1C in Siegel *et al.* 2019 [13])

1.4 The history of GCE of r-process elements

Argast *et al.* (2004) [14] firstly evaluated CCSN and NSM as r-process astrophysical sites from the viewpoint of GCE. In their paper, a very popular problem to consider NSM as r-process sites, was discussed. Neutron star binary (NSB) is formed after two neutron star formation by two CCSNe. The binary will merge by losing their orbital energy by emitting GW. The energy loss rate due to GW is very small and they take very long time to coalesce. The typical time scale is estimated as, at least, 100 million years by the analysis of the binary pulsar observations. Therefore, NSM can not contribute to r-process abundance in an early galaxy and is hard to explain the Europium abundance of metal poor stars, and CCSN was preferred as a r-process astrophysical site in the context of GCE. However, nucleosynthesis simulations suggested that neutrino driven wind from proto-neutron star, a normal type of CCSN model, can produce only light r-process elements (A<130) since the electron fraction Ye becomes not small enough due to neutron destruction by neutrino. Thus, another model of CCSN, MHDJ, was proposed. This type of CCSN is more explosive than the normal one and neutron flux is enough high that all r-process elements are synthesized. However, extremely strong magnetic field, the magnetic energy close to 0.1% of the gravitational energy, is required for such explosion mechanism and the existence itself was suspected.

Hirai *et al.* (2015) [15] performed a chemo-dynamical simulation to take account of the effect of inhomogeneity more precisely. They suggested that if NSM ejecta spread to a region not polluted by Iron enrichment, then NSM can contribute to elemental abundance of metal poor stars.

However, NSM still has another difficulty. Recent observations of double binary pulsars suggested that the distribution of coalescing time (τ_g) is estimated as $dN/d\tau_g \propto \tau_g^{-1}$. The appearance of NSM contribution is delayed from star formation in time τ_g (Beniamini *et al.* 2019 [16]). This distribution function is the same as Type Ia, reported by Totani (2008) [17]. Then, enrichment of r-process elements by NSM and that of Iron by Type Ia are canceled out each other in metal rich epoch and

[X/Fe] should become constant at the late stage of the galaxy. This is inconsistent with the observed Europium abundance in Figure 3 (discussed in Simonetti *et al.* 2019 [18]).

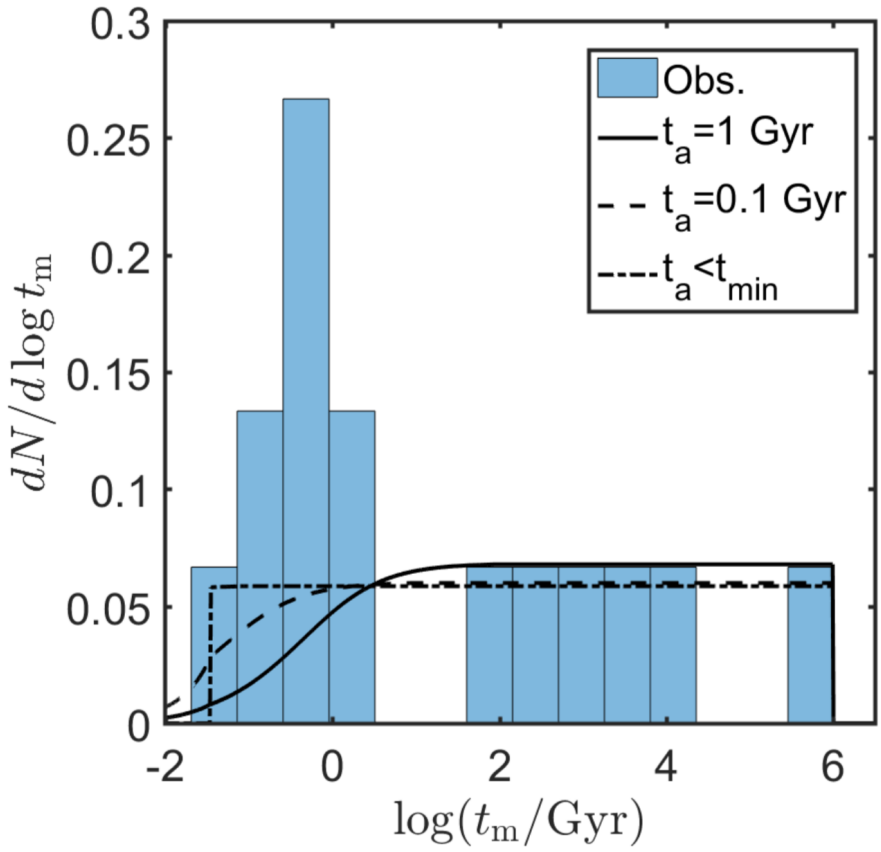

Fig. 8. The observed probability density function of coalescing time (t_m in this figure) reprinted from Beniamini *et al.* (2019) [16]

Recently, another astrophysical site is drawing attention. Collapsars, remaining black holes without supernova explosions, occur just after the end of main sequence lifetime of very massive stars. The event rate of them is very similar to that of CCSNe, but much rarer than CCSNe considering initial mass function with a peak at around one solar mass. Therefore, collapsar can explain the trend of Europium

abundance at both metal rich and metal poor epoch (Siegel *et al.* 2019 [13]).

In this thesis, all of the three components are took into account, We calculate how their contribution has changed in the cosmic/galactic time, confront the evaluated results with observations of elemental abundance in Galactic stars, and propose astronomical observations which help revealing how and where heavy elements have been synthesized and evolved.

2 Theory and Method of The Calculation

2.1 One Zone Galactic Chemical Evolution

One-Zone model describes a simple and standard dynamical and chemical evolution of a Milky Way-like galaxy. In this section, I will review the basic one-zone GCE model established by Timmes *et al.* (1995) [19]. The dynamical evolution in the one-zone model, a model calculates an 'average' evolution of a galaxy, is based on the following four key assumptions.

- A galaxy exchanges materials with the outside of it through gas 'in-flow' and 'out-flow'.
- The star formation rate of a galaxy is determined by gas mass and stellar mass inside it with sufficient precision.
- The time variation is not discrete, but continuous in the calculation.
- The interstellar gas is always well-mixed; a sufficient amount of materials is universally ejected from stellar objects anywhere in the galaxy.

The first and second assumptions are fundamental for GCE calculations and many GCE studies are based on these. The third and fourth assumption is justified in the case that the considered area is sufficiently large and the astronomical phenomena occur sufficiently often The considered area is sufficiently large and the astronomical phenomena occur sufficiently often

2.2 Dynamical Evolution Model

We start by formulating the dynamical evolution of a galactic disk. A galaxy consists of interstellar gas and about two hundreds millions stars.

The total baryonic mass of a galaxy is indicated as the sum of the mass of interstellar gas and the mass of stars within the galaxy. Therefore, total surface density of the galaxy $\sigma_{\rm tot}$

$$\sigma_{\rm tot} = \sigma_{\rm gas} + \sigma_{*} \tag{2-1}$$

2.2.1 Inflow Rate

Galaxies are formed by gas condensation in large scale cosmos. The galactic inflow is assumed to decrease exponentially with time. Therefore, total surface density of the galaxy $\sigma_{\rm tot}$ can be calculated according to the following formula.

$$\dot{\sigma}_{\rm tot}(t) = A\ e^{-t/\tau} \tag{2-2}$$

where τ is the time scale of the disk formation. They took $\tau = 4$ billion years and obtain reasonable results. A is the parameter to adjust the total surface density at the present time; $t = 13.5$ billion years. In this study, we calculated GCE in an one zone similar to the solar vicinity. Therefore, the parameter A was adjusted to reproduce $\dot{\sigma}_{\rm tot}(13.5{\rm Gyr}) = 75\ M_{\odot}/pc^2$.

2.2.2 The Time Evolution of Gas surface density

The galactic inflow purely increases the gas surface density. On the other hand, star formation lead to decrease gas density since stars are formed from interstellar gas and once the gas is trapped in stars, they are no longer interstellar gas. Stellar activities often eject some amount fo gas into surrounding interstellar space. This ejection event enrich the galactic interstellar gas. Thus, the gas surface density is changed by three terms;

$$\dot{\sigma}_{\rm gas}(t) = \dot{\sigma}_{\rm tot}(t) - B(t) + E(t) \tag{2-3}$$

where $B(t)$ and $E(t)$ are star formation rate and ejection rate, the total ejected materials from all the galactic stars in unit of $[M_{\odot}/pc^2]$ respectively.

2.2.3 Star Formation Rate

Star formation is one of the essential activity for the evolution of galactic gas as shown in Eq. (2-3). Stars are formed from interstellar gas, that is, star formation activities consume interstellar gas so that the gas density is decreased. For the galactic disk, the empirical relation between star formation rate and gas surface density is found by Schmidt (1959). In this model, a quadratic Schmidt function is adopted to well reproduce solar composition and elemental evolution of light elements from Hydrogen to Zinc. The star formation rate B is described as follows.

$$B(t) = 2.8\ \sigma_{\rm tot}\ \xi^2_{\rm gas} \tag{2-4}$$

where $\xi^2_{\rm gas}$ is the fraction of the gas in the galaxy, i.e., $\xi_{\rm gas} \equiv \sigma_{\rm gas}/\sigma_{\rm tot}$

2.3 Stellar Recycling

The third term in Eq.(2-3) is the ejection from all the stellar object in the galaxy. After the star formation, stars end their lifetime and eject some materials into interstellar gas. During the entire main sequence phase, the star is relatively quiet and stable. Almost all mass-loss processes occur after the star leaves the main-sequence stellar phase. Stars are in the main sequence phase for more than ninety percent of their lifetime, therefore the delay from star formation to the end of their lives can be approximated by their main sequence lifetime. The main sequence lifetime is a function of their initial mass, hence, the delay from star formation is described by a function of their mass.

In this study, we took data from Weaver and Woosley (1995) [20] for the stars whose mass is less than ten solar mass, and Schaller *et al.* (1992) [21] for stars whose mass is more than ten solar mass. Weaver and Woosley (1995) [20] estimated that

the metallicity effects on main sequence lifetime is about ∼5 %. The lifetime function is shown in Figure 9.

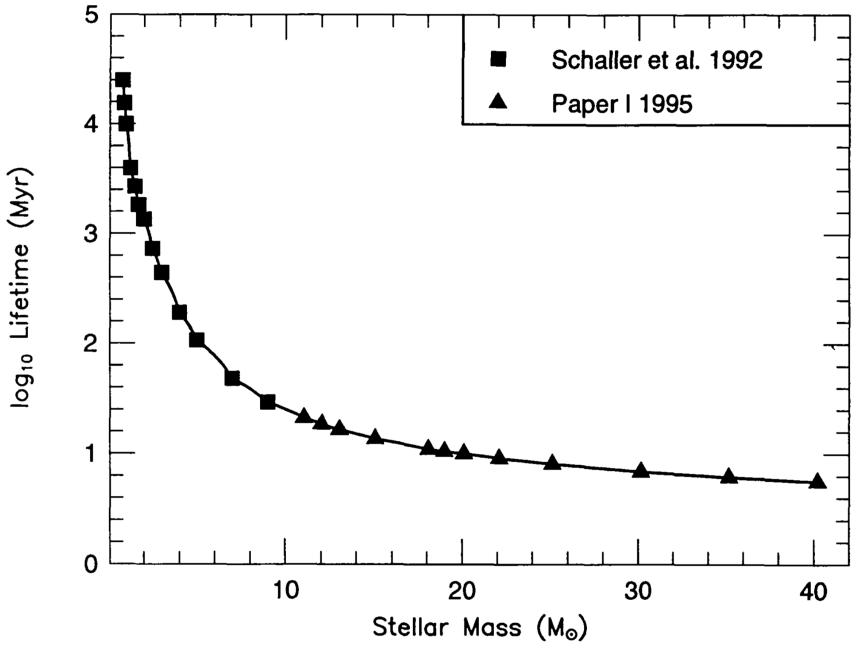

Fig. 9. Main sequence lifetime as a function of initial stellar mass from Weaver and Woosley (1995) [20] and Schaller *et al.* (1992) [21] (reprinted from Timmes *et al.*) [19]

Let us assume that the number of stars in the mass range of $m \sim m+\Delta m$, formed from 1 $M_\odot$ gas is $dn(m)$ at the time t'. These stars end their lives after their main sequence lifetime $\tau(m)$. Thus, the number of stars with mass of m which end their life at the time $t' + \tau(m)$ is

$$dN(m, t' + \tau(m)) = B(t') \cdot dn(m) \tag{2-5}$$

By integrating equation (2-5) over m and variable conversion $t \equiv t' + \tau(m)$, we obtain the number of stars that end their life at time t.

$$N(t) = \int B(t-\tau(m)) \cdot dn(m)$$
$$= \int B(t-\tau(m)) \cdot \frac{dn}{dm}\, dm \qquad (2\text{-}6)$$

The second term in equation (2-6) is the initial mass function $\phi(m)$. We took it from Kroupa (2001) shown in Figure 10

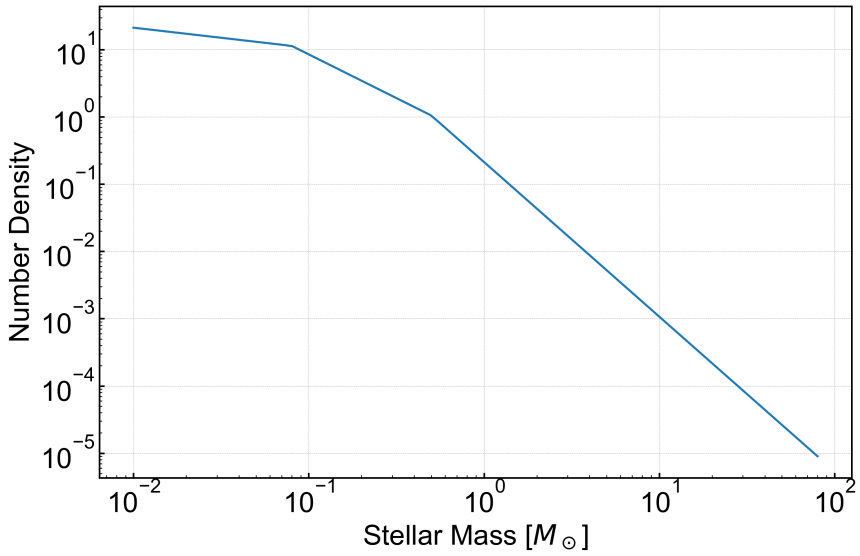

Fig. 10. Initial Mass Function based on Kroupa (2001) [22].

The elements newly formed in main sequence stars are partially ejected into interstellar gas and stars are formed from this enriched gas. This repeated process is called *stellar recycling*.

Hence, for the density of non-primordial elements, i.e., heavier than Boron, the time derivative of surface density σ_i of nuclei with mass number i, can be described as follows.

$$\dot{\sigma}_{\rm i}(t) = Eject - Birth \tag{2-7}$$

$$= \int B(t-\tau(m))\ \phi(m)\ E_i(m)\ dm - B(t)\ \frac{\sigma_{\rm i}}{\sigma_{\rm gas}} \tag{2-8}$$

The first term describes the enrichment due to the ejection from stars at the end of their main sequence stages, while the second term describes the disappearance of isotopes from the gas by the confinement in stars due to the star formation. $E_i(m)$ is the mass of nuclei with a mass number i ejected from stars at the end of their main sequence lifetime.

If an astrophysical event occurs immediately after the 'death' of a main sequence star, the rate of such astrophysical events can be approximated by 'death rate' of main sequence stars in equation (2-6). CCSN is one of the most vital representatives. Therefore, the event rate $R_{\rm CCSN}$ of CCSN is described as follows.

$$R_{\rm CCSN} = \int_8^{40} B(t-\tau(m))\ \phi(m)\ dm \tag{2-9}$$

2.4 Binary Systems

To discuss the galactic evolution with metallicity [Fe/H]<-1, the contribution from Type Ia is negligible since they are the source of Iron especially at high metal era ([Fe/H] > -1).

Timmes *et al.* (1995) [19] firstly introduced a novel formula to describe the elemental enrichment by Type Ia supernovae which can take account of binary scenario. They assume the birth rate of a binary system with masses of m_1 and m_2 ($m_1 \geq m_2$) is proportional to an initial mass function for single stars with mass of $M(\equiv m_1+m_2)$. Using this assumption, they formulate the event rate $R_{\rm Ia}$ of Type Ia supernovae as follows.

$$R_{\rm Ia}(t) \;=\; C \int_3^{16} \int_{q_{\rm M}}^{0.5} B(t-\tau(m_2))\;\phi(M)\;P(q)\;dq\;dM \qquad (2\text{-}10)$$

where q is the mass ratio of the secondary to total, i.e., $q \equiv m_2/M$. C is a parameter which adjusts the amplitude of the Type Ia contribution, set to be 0.007 in Timmes *et al.* (1995) [19].

We extended this equation and formulate the event rate of NSM taking account of their coalescing time. Neutron star binary lose their orbital energy by emitting gravitational wave and finally merge as NSM. The merging delay time τ is a function of the initial binary separation a, and analytically calculated by the general theory of relativity.

$$\tau_{\rm g}(a) \;\propto\; a^4 \qquad (2\text{-}11)$$

The delay from star formation of NSM is $\tau(m) + \tau_{\rm g}(a)$. Then, we obtain the formula for NSM rate as follows.

$$R_{\rm NSM} \;=\; \epsilon_{\rm NSM} \iiint_{M_{\rm l}}^{M_{\rm h}} B(t \;-\; \tau(m_2) \;-\; \tau_{\rm g}(a))\;\phi(M)\;P_{\rm a}(a)\;P_{\rm q}(q)\;dM\;dq\;da \qquad (2\text{-}12)$$

where ϵ_{NSM} is the fraction of massive stars which form neutron star binaries, a parameter which can adjust the amplitude of NSM contribution.

$P_{\rm a}(a)$ and $P_{\rm q}(q)$ are the probability density functions of a and binary mass ratio q, respectively.

$P(a)$ is assumed to be proportional to a^{-1}. It lead to the probability density function of $\tau_{\rm g}$ that proportional to ${\tau_{\rm g}}^{-1}$. This trend can be seen in Galactic field binary neutron stars. The distribution of $\tau_{\rm g}$ is estimated from observation of binary pulsar as discussed in Beniamini and Piran (2019) [16]. The observed distribution is shown in Figure 8.

Event rate of collapsar is described by the same integral as CCSN. Differences are 1. a scale factor $\epsilon_{\rm COL}$ is added, and 2. the lower limit of integration with respect to mass is set to be 40.

$$R_{\rm COL} \;=\; \epsilon_{\rm COL} \int_{40} B(t-\tau(m))\ \Psi(m)\ dm \tag{2-13}$$

We take into account of these three r-process component simultaneously. Therefore, the enrichment event rate of r-process elements is described as follows.

$$\dot{\sigma}_{\rm i}(t) = \sum_{*}(R_*\ E_{{\rm i},*}) \;-\; B(t)\ \frac{\sigma_{\rm i}}{\sigma_{\rm gas}} \tag{2-14}$$

summation over r-process astrophysical sites $*$(: CCSN, NSM and COL).

For the analysis of p-isotopes in this thesis, we calculated the evolution of nuclei produced by Type IA, CCSN and collapsar. The s-process contribution is taken from other study. We use the result of Kobayashi et al. 2020 [23].

2.5 Calculated Gas and Metallicity Evolution

Before describing our detailed r-process GCE, we present the fundamental calculation result on the evolution of galaxy. The surface density is one of the most essential parameter of GCE simulation. The star formation rate is dependent on this value and has an impact on event rates of nucleosynthetic events.

Figure 11 shows the evolution of total surface density of a galaxy.

We tried some parameters or models of r-process nucleosynthesis, since the amount of r-process elements produced by a certain astrophysical site $E_{i,*}$ is not still clear, However, the fraction of r-process elements in the interstellar gas is less than 0.01% and such a tiny amount of r-process elements does not affect gas evolution in the galaxy so much. Therefore, the variation of gas evolution due to model selection is so small that only one result of gas evolution is shown here.

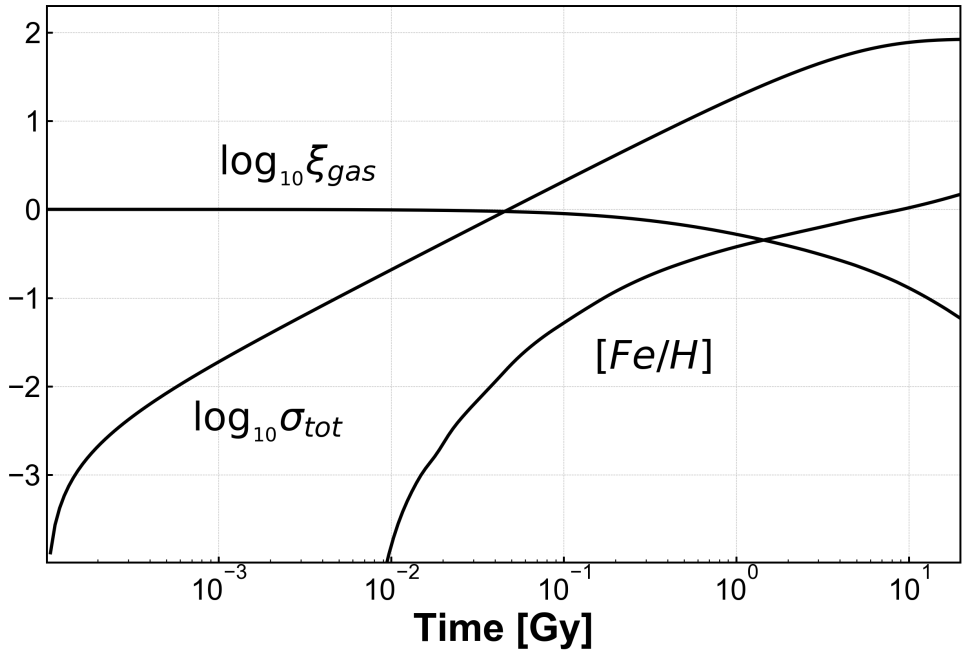

Fig. 11. The time evolution of total surface density σ_{tot} $[M_\odot/pc^2]$, gas fraction ξ_{gas} and metallicity [Fe/H].

With this assumption, we can obtain another expression of the differential equation (2-14) for $\sigma_{\mathrm{i},*}$, a surface density of nuclei with mass number i originating from a certain astrophysical site $*$, an ingredient of σ_{i}.

$$\dot{\sigma}_{\mathrm{i},*}(t) \;=\; R_* \; E_{\mathrm{i},*} \;-\; B(t) \; \frac{\sigma_{\mathrm{i}}}{\sigma_{\mathrm{gas}}} \tag{2-15}$$

$$\Leftrightarrow \quad \left(\frac{B(t)}{\sigma_{\mathrm{gas}}(t)} + \frac{d}{dt} \right) \frac{\sigma_{\mathrm{i},*}(t)}{E_{\mathrm{i},*}} \;=\; R_{\mathrm{i}}(t) \tag{2-16}$$

The values of $E_{\mathrm{i},*}$ are different between models a-c, however, the solutions of $\sigma_{\mathrm{i},*}(t)$ and $R_*(t)$ are just scaled, in other words, the time dependency is common.

Therefore, the event rate or surface density of certain nuclei normalized by the value at [Fe/H]=0 is independent from model selection or nucleosynthesis simulation results ($E_{\mathrm{i},*}$).

2.6 Calculated Event Rate of Astrophysical Events

A set of the event rates is shown in Figure 12. Collapsars appear first since the mass of their progenitor is more than 40 solar mass. After collapsar, CCSNe follow and NSM occurs in the last. The timing of NSM emergence is dependent on their minimum coalescing time scale (τ_g in equation 2-12). In the case of minimum coalescing time is one million years, NSM can occur before [Fe/H]=-3. If the minimum coalescing time is maximum (100 million years), NSMs occur in only [Fe/H]>-1.2.

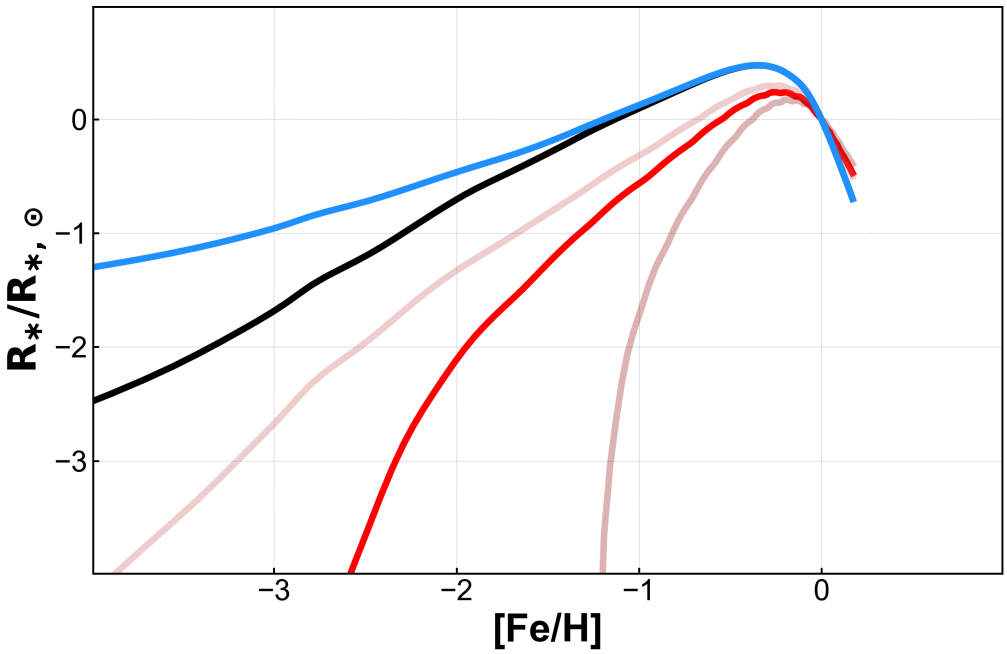

Fig. 12. The evolution of Event Rate normalized by the value at [Fe/H]=0. The blue and black lines show the event rate of collapsar and CCSN respectively. Three red lines show NSM event rate of different minimum coalescing time. τ_g=1, 10 and 100 million years are taken from light to dark.

The contribution of a site $*$, f_*, is defined as the total amount of r-process elements originating from a site $*$.

$$f_* \equiv \sum_i \sigma_{\mathrm{i},*} \tag{2-17}$$

Since a fraction of nuclei i is time-independent, the time dependency of f_* is the same as that of $\sigma_{\mathrm{i},*}$. Therefore, the normalized history of contributions from site i is also independent from model selection (shown in Figure 13). To compare with observed elemental abundance in the galactic stars, the ratio to Iron abundance is taken.

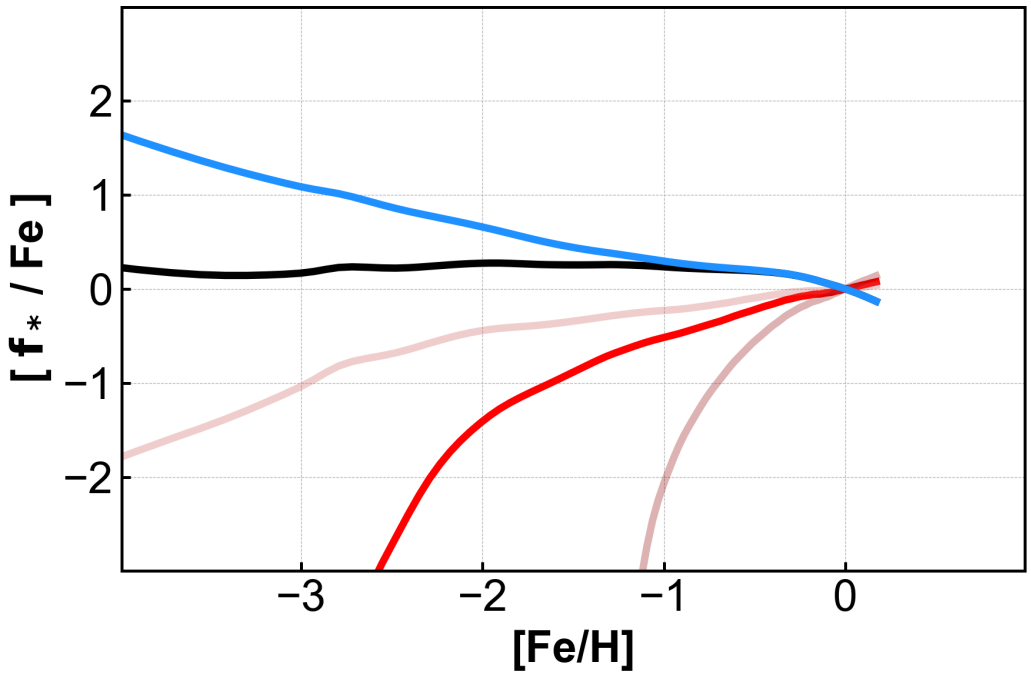

Fig. 13. The evolution of contribution from each sites normalized by the value at [Fe/H]=0. The colors are same as Figure 12

The iron abundance comes from CCSNe in metal poor epoch, therefore, $[f_*/\mathrm{Fe}]$ is almost same as $[f_*/f_{\mathrm{CCSN}}]$. In the early galaxy, collapsar contribution was larger than that in solar abundance, and NSM contribution was much smaller.

In the late time, collapsar contribution is almost same as that of CCSN. The NSM

contribution becomes almost flat as already mentioned in previous studies [24].

3 Our GCE Calculation for r-process Elements

3.1 The r-process abundance pattern by each nucleosynthesis site

3.1.1 Supernovae

We have considered two well-known types of core-collapse supernovae, NDWs and MHDJs. NDWs are associated with typical core-collapse supernovae. In this study, we adopted the calculated r-process yield in the NDW of Wanajo (2013) [6], a protoneutron star with $1.8M_{\odot}$.

MHDJs are a rare type of supernova compared to NDWs, but this type of supernova produces a very large amount of r-process elements, as much as $10^{-4}M_{\odot}$ (about $10^{-6}M_{\odot}$ for NDWs). Since the contribution to the overall GCE is the product of the frequency of events and the yield per event, MHDJ can affect the evolution of heavy elements in the Galaxy. The model yields for MHDJ are taken from [8].

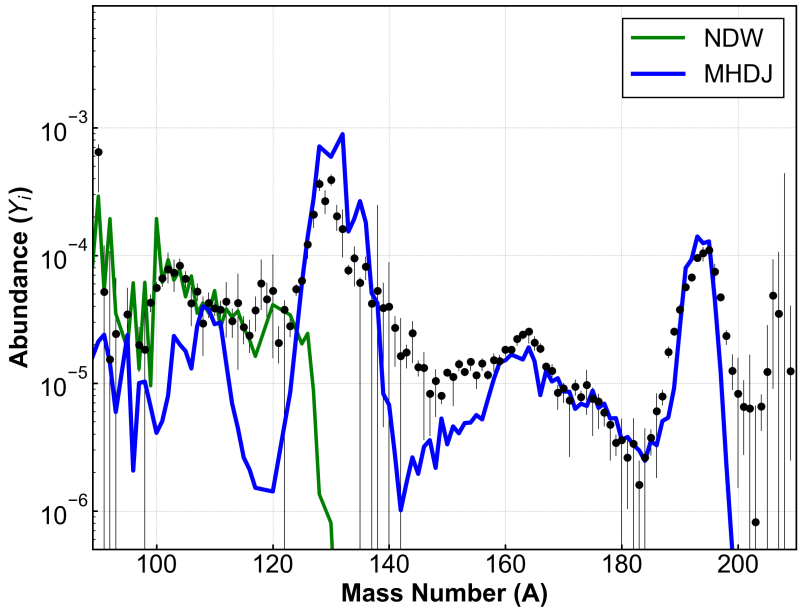

Fig. 14. The abundance pattern of r-process yields produced by NDW(green) and MHDJ(blue)

3.1.2 Collapsar

Collapsar is an object in which a black hole is formed by gravitational collapse. The corresponding astronomical phenomena are still unclear. There are two possible observed events; SLSN and failed supernova. For the collapsar model, we adopt a version of Nakamura et al. (2015) [11] modified by Famiano et al. (2020) [25]. We also adopted another model by Siegel et al.(2019) [13]. Their model is associated with hypernova explosion. See section 1.3.4 for the details of these models.

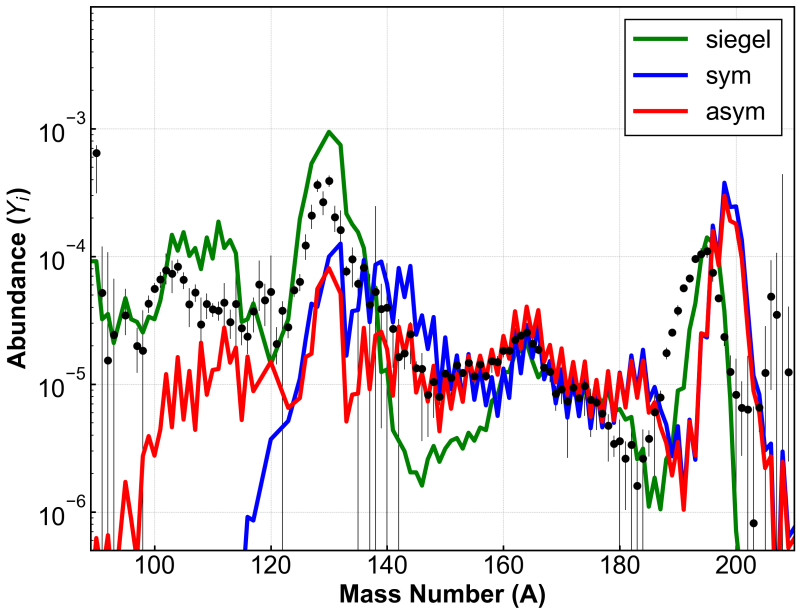

Fig. 15. The abundance pattern of r-process yields produced by two collapsar models. The green line shows the final abundance of a collapsar model of Siegel et al.(2019) [13]. The blue and red lines a taken from Famiano et al.(2020) [25] The blue is the case that symmetric FFD is adopted, while asymmetric FFD is used for the red.

3.1.3 Neutron Star Merger

Neutron star merger is a promising site for r-process nucleosynthesis. NSM is a merger event of two neutron star. This phenomenon is anisotropic and explosive. Around the merging binary system, the physical condition varies in space and time. The end point of r-process depends on the neutron fraction and dynamical time scale. Thus, neutron star merger has several components of ejecta.

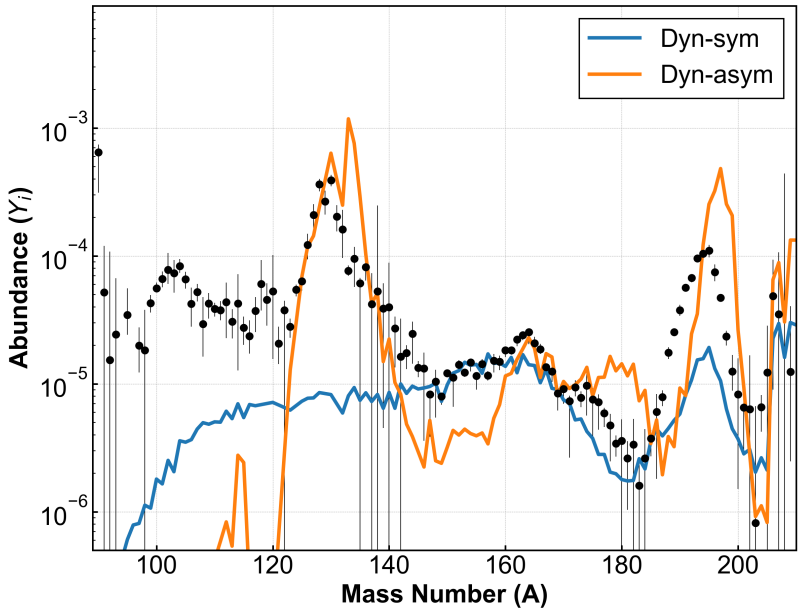

Fig. 16. The abundance patterns of r-process yields of NSM. The blue and orange lines show the calculated results adopting symmetric FFD (Suzuki et al. 2018) and asymmetric FFD (Shibagaki et al. 2016) respectively.

3.2 The Calculation Configuration and Parameters

3.2.1 The Combination of r-process sites

We should choose a set of stellar models of each r-process site in order to calculate equation (2-14). Model selection is one of the most essential input of our calculation, since it determines the main contributor to a certain element. There are two obvious constraint on this model selection even before performing any GCE calculation.

1. All considered elements, the r-process elements in this section, should be produced in, at least, one of the selected astrophysical sites
2. Solar system abundance pattern should be well reproduced.

From the first constraint on combinations of models for r-process astrophysical sites, we choose three possible combinations.

NDWs from nascent neutron stars are promising sites for the production of light r-process elements (A< 120). Wanajo (2013) calculated NDW with $1.8M_{\odot}$ progenitor mass and suggested that neutron flux is not high to produce heavy r-process elements. In this model, r-process stops before reaching to the second peak, i.e., proceeds up to mass number A$\approx$ 130. The detailed pattern is shown by the green line in Figure 14

The MHDJ supernova is the most reasonable site for the second peak of the well-known r-process. MHDJ model by Nishimura *et al.* (2012) [8] produces all r-process elements except for super massive nuclei heavier than the third peak as the blue line shown in Figure 14

The NSM tidal ejecta is also an ideal site for the production of heavier r-process nuclei, since NSM ejects so large amounts of neutrons ($Ye < 0.4$). The r-process in NSMs can reach into the supermassive nuclei. Hence, the distribution of fission fragment of such massive nuclei has a very large impact on the results of nucleosynthesis in the ejecta from NSMs. Suzuki et al. (2018) [10] and Shibagaki et al. (2016) [5] performed nucleosynthesis calculations for the same ejecta flow from a NSM with symmetric FFD and asymmetric FFD. We adopted these two model using different nuclear physics input.

In reality, NSM have both of disk and dynamical ejecta, however, the mass ratio between them is still not clear. Since the purpose of this study is not to determine NSM parameters which can reproduce observed abundance but to obtain some constraint on r-process among several astrophysical sites or to suggest a possible time evolution of r-process elements. We focused on the dynamical ejecta from NSM in this thesis. This strategy is also justified by the analysis of Sr evolution explained in the result section. The analysis imply that the contribution from NSM should be relatively small for the light r-process elements. The disk ejecta of NSMs produce only lighter r-process elements compared with the dynamical ejecta. Therefore, this type of ejecta does not have not a large impact on GCE even though Sr is do observed by NSM observation [26].

The collapsar is also an attracting astrophysical site as a source of r-process nuclei. The collapsar means the astrophysical object which is originally a single massive star and collapsing into a black hole without a remaining neutron star. However, associated observable phenomena for this object is still not clear since the theoretical calculation of collapsing massive star is hard. Two astrophysical phenomena with observational counterparts are suggested; super-luminous supernovae and failed supernovae. We considered both cases. Model 1 assumes that the collapsing star is a failed supernova. For this, we adopt a modified version of the collapsar r-process model of Nakamura et al. (2015) (Famiano et al. 2020). In this case, the MHDJ SNe is the source of the SLSNe; in the second model (Model 2), the collapsar is assumed to be the SLSNe. For this, we adopt a model from Siegel et al. [13].

Thus, we consider, in total, four cases of model combination, two as nuclear physics inputs of FFD and two as collapser models. Model combinations are summarized in Table 1.

3.2.2 The scale parameters ϵ_{NSM} and ϵ_{coll}

The efficiency parameters ϵ_{NSM} and ϵ_{col} in Eq. (2-12) and Eq. (2-13) are free parameters adjusted to best fit the event rate of each site and the abundance pattern of the r-process [Fe/H]=0 at the present time. The event rate of SNe in the Galaxy

Table 1. The model combination

	symmetric		asymmetric	
	(Model 1-s)		(Model 1-a)	
Failed SN	NSM	Suzuki et al.	NSM	Shibagaki et al.
	Collapsar	Famiano et al.(1)	Collapsar	Famiano et al.(2)
	(Model 2-s)		(Model 2-a)	
Hypernova	NSM	Suzuki et al.	NSM	Shibagaki et al.
	Collapsar	Siegel et al.	Collapsar	Siegel et al.

has been well studied. Recently, the frequency of NSMs has also been estimated by detecting GWs and short gamma-ray bursts (SGRBs) [27]. The composition of the solar system is the only object for which detailed patterns of isotopic abundance ratios have been measured. Precise and sophisticated analyses of meteorites, led by RIKEN, have measured the abundance ratios of various species within an error range of < 0.1dex.

The calculated ϵ_{NSM} and ϵ_{coll} are determined to best reproduce the solar system abundance ratios.

4 The Result and Discussions on r-process GCE

4.1 The Time Evolution of the r-process Abundance Pattern

4.1.1 General features of the abundance patterns

First of all, we discuss several features of our calculated solar abundance pattern which was obtained by using the yields from four considered astrophysical sites at solar metallicity (the top panels in Figure 17, 18).

Although the MHDJ r-process (green line in Figure 17, 18) explains well the abundance peaks around $A \sim 130$ and 195 and the hill of lanthanides around $A \sim 165$, a deficiency of isotopes around $A = 140 \sim 145$ remains in either model. Indeed, most r-process nucleosynthesis calculations underproduce the heavier isotopes just above the second peak [28]. If the r-process reaches the superheavy nuclei, the second peak is broadened by fission recycling.

The NSM and collapsar abundances may avoid the lack of production around $A = 140 - 160$ seen in many prior r-process calculations [28]. Famiano's collapsar model in Figure 17 and the NSM model with asymmetric FFD in the right panel of Figure 18 compensate this lack. This is because the r-process in a very neutron-rich environment can increase the amount of fission fragments present at $A \approx 130 - 150$ due to the many fission recycling cycles.

The tidal component of the NSM dynamic ejecta has a very low electron fraction ($Y_e \sim 0.1$). Therefore, the r-process pathway will run along an extremely neutron-rich isotope. The reaction stream quickly reaches the heavier fissile nuclides in the $A = 250-290$ region. Thus, the FFD strongly affects the mass range of $A = 100-180$ and the final abundance distribution of heavier isotopes [5]. Using a symmetric

FFD [10] for the NSM r-process, Figure 17 and Figure 18 on the left, the second peak around $A \sim 130$ is reasonably reproduced, while an asymmetric FFD [5] model on the right shows a smoothing of the abundance distribution. This may solve a longstanding problem in r-process nucleosynthesis, the underproduction of $A = 140 - 145$ nuclides as discussed above.

However, regardless of the FFD selection, the third peak was found to shift slightly into the heavy mass region. This is because the neutron number density remains high after freezing due to tidal ejection from the NSM. In addition to these features, another feature that is attributed to the high-entropy environment is the appearance of odd-even patterns in the abundance of lanthanides. This is a typical feature due to very fast neutron capture and sudden freeze-outs. However, we note that the Siegel et al. (2019) [13] calculations employ a different ejecta model and show a smoother pattern (Figure 18).

The collapsar r-process yield shows a variation which depends on the models just as the CCSN and neutron star merger r-process do. Motivated by the first hydrodynamic collapsar model of Macfadyen et al. (1999) [29], Surman et al. (2006) [30] studied the r-process nucleosynthesis. They noted that the representative disk accretion rates produced by the MacFadyan-Woosley's collapsar model are too low to produce enough r-process elements and suggested that more rapidly accreting disks or higher black hole spins might make suitable conditions for the r-process. Our collapsar model [11] adopted in the present study for a successful r-process is calculated by a relativistic axisymmetric MHD code and applied to the collapse of rotating magnetic massive stars [31, 32]. We extensively studied the collapsar r-process by explicitly taking account of the effects of the magnetic field and nuclear fission [25] and found interesting variation in the r-process yields. Siegel et al. (2019) [13] also carried out a similar but different collapsar model calculations for a successful r-process. As such, the collapsar model has progressively evolved in numerical simulations and resultant nucleosynthesis. Once one makes a collapsar model with successful r-process nucleosynthesis, the basic properties such as large ejected mass and reasonable abundance pattern over the entire mass region up to the 3rd peak elements are more or

less similar to each other although the details are still different. Therefore, our core conclusion concerning the collapsar contribution to the GCE of r-process elements does not significantly change when considering this uncertainty.

4.1.2 The time evolution of isotopic abundance pattern

Our simple GCE model indicates a time-metallicity relation given by $t/10^{10}y \approx 10^{[Fe/H]}$. However, this relation is broken in the extremely metal-deficient region [Fe/H]<-2 because of the inhomogenity of the early Galaxy due to the stochastic Galactic star formation [15] at low metallicity. Nevertheless, metallicity is a reasonable measure of the time evolution of the Galaxy for [Fe/H]>-2. Differences in the time delay from star formation to nucleosynthesis lead to variations in the isotopic r-process abundance patterns with metallicity. In general, the delay is shortest for collapsars and longest for NSMs. Therefore, galaxies in the early universe have a large contribution from collapsars, while the contribution from the NSMs is largest at the present time.

Figures 17 and 18 show examples of the difference between the metallicity function of the abundance mass distribution and the FFD for both *model 1* (Figure 17) and *model 2* (Figure 18). The lines in the figure correspond to the NSM contribution (red line), the collapsar contribution (blue line), and the CCSNe contribution (green line). The fit of the total abundance to the solar r-process composition is shown by the black line.

The abundance distributions from these four different r-process sites have unique features, especially for nuclides heavier than the first r-process peak at A=80. NDWs produce only lighter r-process elements in the $A < 130$ mass range. On the other hand, the MHDJ produces elements with r-process abundance peaks, especially around the second and third peaks at $A \approx$130, 195. The contributions from CCSNe, i.e. the sums of NDW and MHDJ, are shown as green lines in the figures.

Before discussing the details of abundance patterns, we describe the general trend of time evolution of our calculated results. Figures 17 (for *Model 1-s* and *Model 1-a*) and 18 (for *Model 2-s* and *Model 2-a*) highlight the fact that among these possible astrophysical sites, CCSNe (i.e. NDW and MHDJ) and collapsars make the predominant contribution in the early Galaxy. On the other hand, the NSM contribution is negligible for early galaxies, reaching the late stages of galaxy evolution due to the

long merging time delay τ_g. The NSM contribution grows gradually with increasing metallicity and eventually reaches 1 % of the total abundance of solar r-process elements at [Fe/H] = -1.5, -1.3, and -0.7 for models with a minimum coalescence times of τ_g= 1, 10, and 100 My, respectively. In the cases that adopt the symmetric FFD, NSMs change the total abundance pattern only slightly when the Galaxy has evolved to near solar metallicity [Fe/H]=0. This is because the NSM contribution fraction is only about 1%.

Korobkin et al. (2020) [33] discussed the change in ejecta mass due to different tidal ejecta models and displayed their impact on abundance patterns. These differences lead to slight differences in the abundance pattern of the r-process, but only within <0.3 dex. The dependence of the merger rate on metallicity was also discussed. Figures 21, 22 in the next section show that the NS merger contribution appears only partially at high metallicities due to cosmologically long merger times and the predominance of collapsars and MHDJ CCSNe in the full metallicity region. Therefore, we conclude that the dependence of the model on the variation in ejected mass of mergers does not dramatically change our core results in GCE for the r-process abundance patterns shown in Figures 17-22. This conclusion is also nearly independent of the model selection of astrophysical sites and input nuclear physics.

Moreover, although the NSM receives r-process contributions not only from tidal ejecta but also from accretion disk outflows as neutrino-driven winds, we focus here on dynamical tidal ejecta as in Kajino et al. (2019) [28] and use the Koroblin et al. (2012) [34] using 30 outflow trajectories based on outflow trajectory simulations [34, 35, 36]. These trajectories are based on SPH simulations under Newtonian gravity, and neutrino transport is considered in the neutrino leakage scheme [37].

Numerical simulations provide increasing evidence that both wind and jet outflow components contribute to r-process nucleosynthesis [9]. These components strongly affect the lighter r-process elements, including the first peak, but produce fewer hills of heavier elements and rare earth elements above the second and third peaks [38]. In fact, it may be possible to change the abundance ratio of nuclei in A< 120 in the r-process abundance pattern. However, in this light mass region (A < 120), the

NDW from CCSNe is dominant so that the variation due to NSM model selection is expected to be negligibly small in our model calculations. We note again that the NSM r-process is highly dependent on the ejecta model and input nuclear physics.

The detailed time variation of the abundance pattern does depend on the input nuclear physics and/or models of the ejecta used in the r-process simulations. A typical example of the dependence on input nuclear physics is the FFD. As discussed previously, symmetric and asymmetric FFDs can lead to very different abundance patterns over the entire mass range. The left panels show the case of a symmetric FFD and the right panels are for an asymmetric FFD.

In the metal-deficient region [Fe/H]< -1.5, the NSM contribution does not change the total pattern because the r-process abundances are dominated by CCSNe and/or collapsars. On the other hand, the abundance pattern changes drastically as a function of metallicity for [Fe/H] < -1.5. Figure 17 exhibits a very busy abundance pattern because of the odd-even structure in the collapsar r-process yields. There are significant shifts of the second and third peaks towards heavier mass numbers as shown by the black lines. This is because both the collapsar and NSM r-processes shift the peaks towards the heavier mass region.

It is essentially important that the time evolution in isotopic abundance patterns originates from very different time delays between collapsars (or CCSNe) and NSMs, i.e. different timescales from the formation of progenitor stars until the explosive nucleosynthesis. Here, we summarize the features of collapsar abundance pattern which predominates the abundance pattern in metal poor epoch in the Models 1-s and 1-a.

The abundance pattern in the collapsar r-process (blue line in Figure 17) has three unique features due to the very rapid-neutron captures caused by the relatively high values of the neutron density at freezeout [25]. First, the r-process peaks are shifted systematically towards the heavier mass region. This is caused by residual neutron captures during β-decay after freezeout of the r-process. This causes a discrepancy away from the observed solar r-process abundance pattern around the third peak $A \sim 195$ (Figure 17). Secondly, an odd-even pattern manifests in the lanthanide

abundance hill. This is a typical feature resulting from very rapid-neutron captures and the sudden freezeout. We note, however, that in the Model 2-s and Model 2-a, a smoother pattern of Siegel et al. [13] is adopted. Thirdly, the second peak in the collapsar model is broadened to higher mass region A= $140 - 150$ as mentioned previously.

The properties of neutron-rich unstable nuclei and the physical conditions of the trajectory dynamics are thus intricately connected in any nucleosynthesis simulations. However, if some characteristic features, such as those discussed here, were measured in the isotopic abundances of r-process enhanced metal-deficient stars, this could confirm that the heavy nuclei in those stars originate from a single or a few very similar r-process events. Unfortunately, so-called universality in elemental abundance pattern does not exhibit clearly a single r-process site as to be discussed later.

The abundance pattern in Model 2-s shows the lack of A=$140 - 160$ in any mettalicity. This is because both NSM and collapsar can not produce amounts of these elements in this mass region. The symmetric FFD in NSM leads to high second and third peak elements but relatively small abundance of the nuclides just above the peaks. Also, the collapsar model of Siegel et al. (2019) underproduces these nuclides. On the other hand, the abundance pattern of Model 2-a very well describes the solar system abundance pattern around A=$140 - 160$. NSM yields significantly enhance the nuclides in this mass region by the daughter nuclei from fission. These specific features of abundance patterns in different astrophysical sites are expected to manifest themselves clearly in the time evolution of the abundance pattern. Our theoretical predictions could be tested in future elaborate analyses of spectroscopic observations of halo stars with various metallicities.

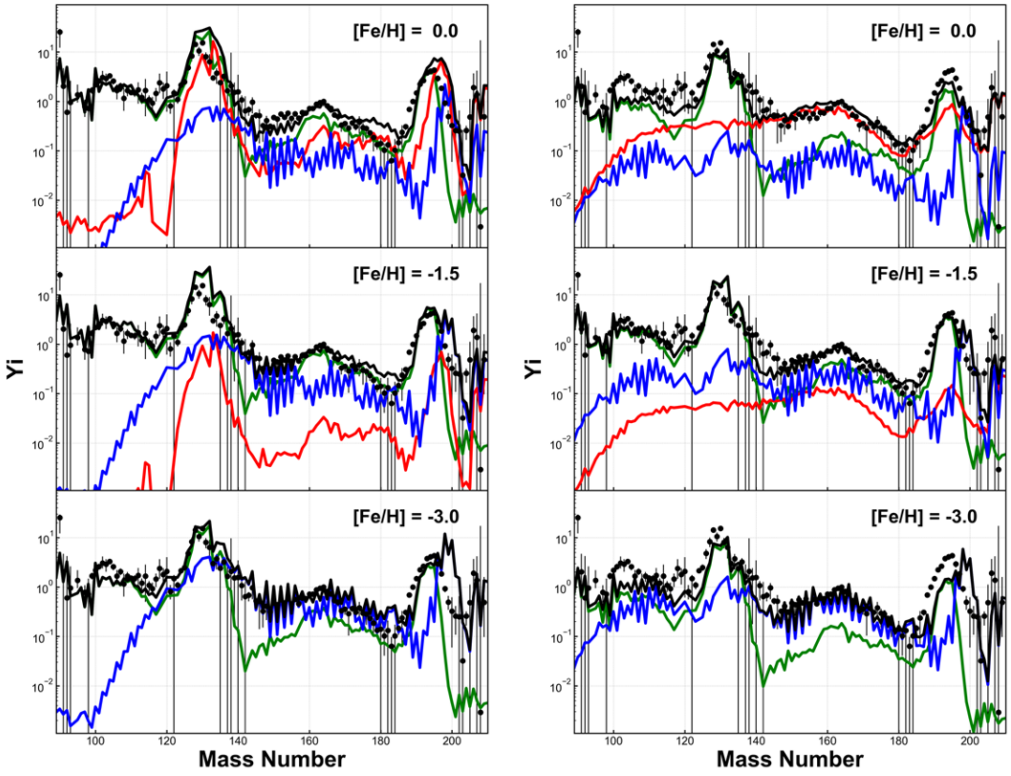

Fig. 17. The isotopic abundance pattern in the case of Model 1-s and Model 1-a. The updated version of Fig. 1 in Yamazaki et al. (2022) [39]

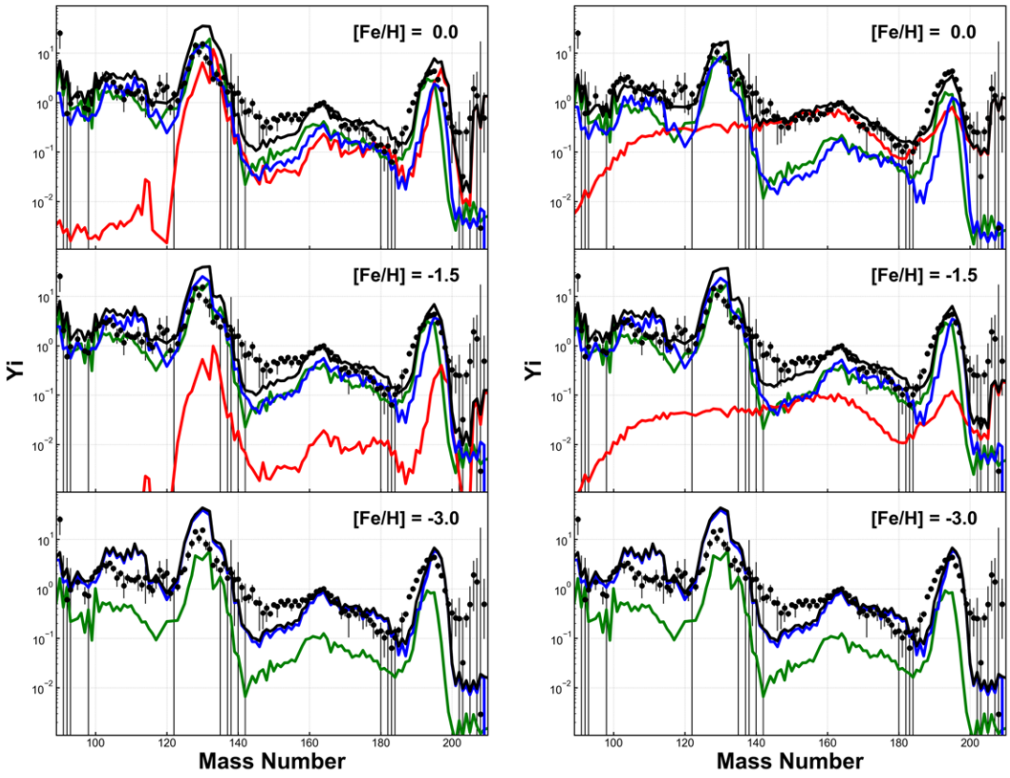

Fig. 18. The isotopic abundance pattern in the case of Model 2-s and Model 2-a. The updated version of Fig. 2 in Yamazaki et al. (2022) [39]

4.1.3 Elemental Abundance pattern

Figure 19 displays the calculated elemental abundance patterns as a function of atomic number Z in *Model 1-s* , symmetric FFD is adopted, (a) and *Model 1-a*, asymmetric FFD is adopted, (b) compared with observational data in r-process enhanced metal-poor halo stars, BD+173248 ([Fe/H] = -2.1) [40] and CS22892-052 ([Fe/H] = -3.1) [41]. Figure 20 is a similar figure but for *Model 2-s* and *Model 2-a*. They exhibit a more or less similar elemental abundance pattern for any metallicity.

In particular, around the lanthanide hill near Dy (Z=66), they agree with each other independently of any models. This feature is known as the universality of the r-process elemental abundance pattern [1] previously introduced in section 1.1.1. Such similarity is due to the fact that there are many isotopes contributing to the same atomic number Z with different mass numbers A [5]. Moreover, this fact enable us to consider multiple astrophysical sites in GCE calculation, without violating the r-process universality in elemental abundance pattern, that naturally change the isotopic abundance pattern of r-process elements.

The peak height around Te (Z=52) and Os (Z=78) depends on the models. This model dependence arises from the different contribution fractions from the four astrophysical sites. Unfortunately, the second peak elements except for Te [40] have not been observed in metal-deficient halo stars.

Most of the nucleosynsthesis calculations with any ejecta model shows a discrepancy near Z=57-60 [5, 28]. It manifests as a deficiency in the A-distribution above the second peak $A \sim 130$ in Figure 19. The only exception is the NSM model with an asymmetric FFD and the Famiano's collapsar model which we adopted. In these ejecta models, the effect of fission recycling smooths abundance distribution over the entire mass region $A > 100$ [5]. The most abundant isotopes smooth the detailed structure apparent in the mass distributions of Figure 19, then the underproduction does not appear in our model because of collapsar contribution. Thus, this discrepancy might not be due to the astronomy; observations or model of galactic evolution, but rather to the theoretical calculations, astrophysical hydrodynamic simulations or

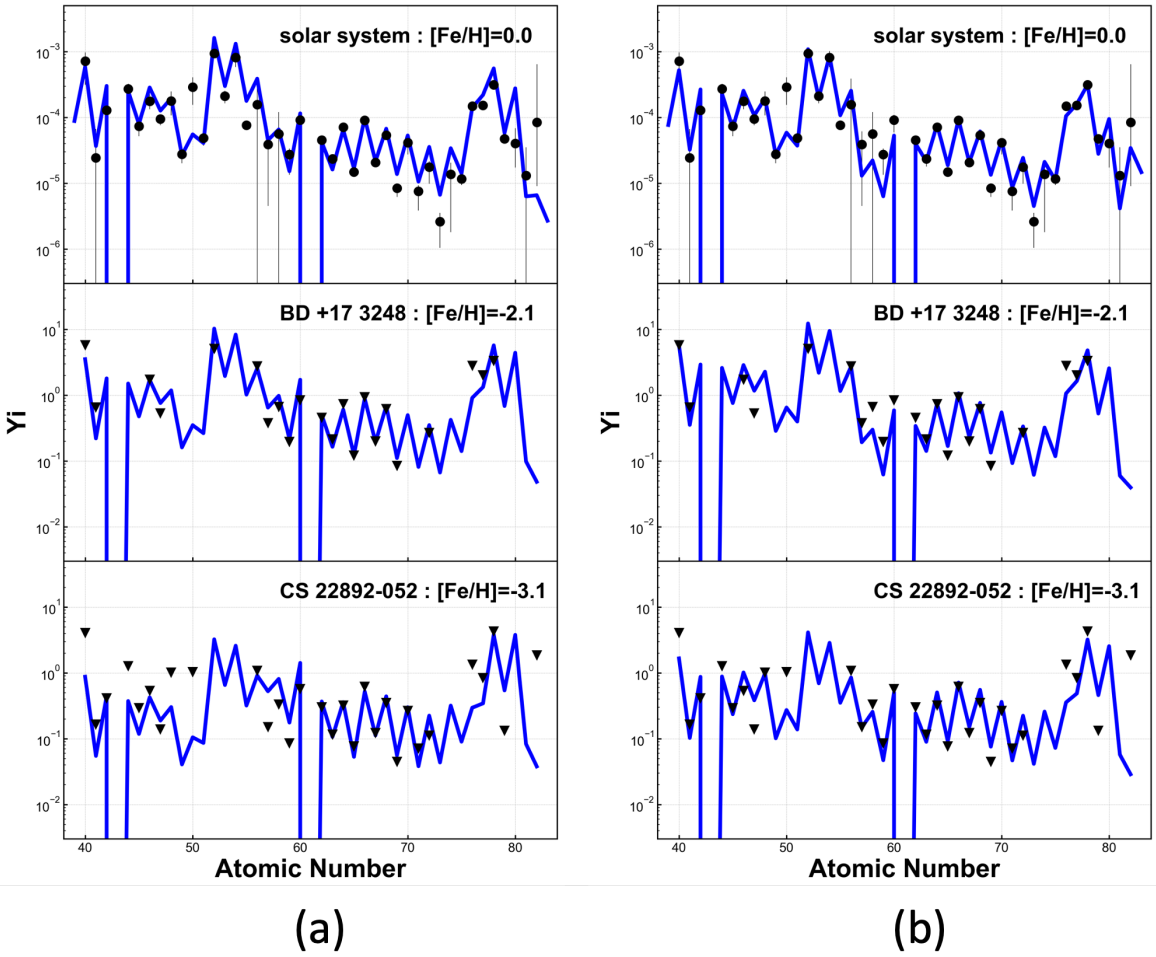

Fig. 19. The elemental abundance pattern in the case of Model 1-s and Model 1-a. The updated version of Fig. 3 in Yamazaki et al. (2022) [39]

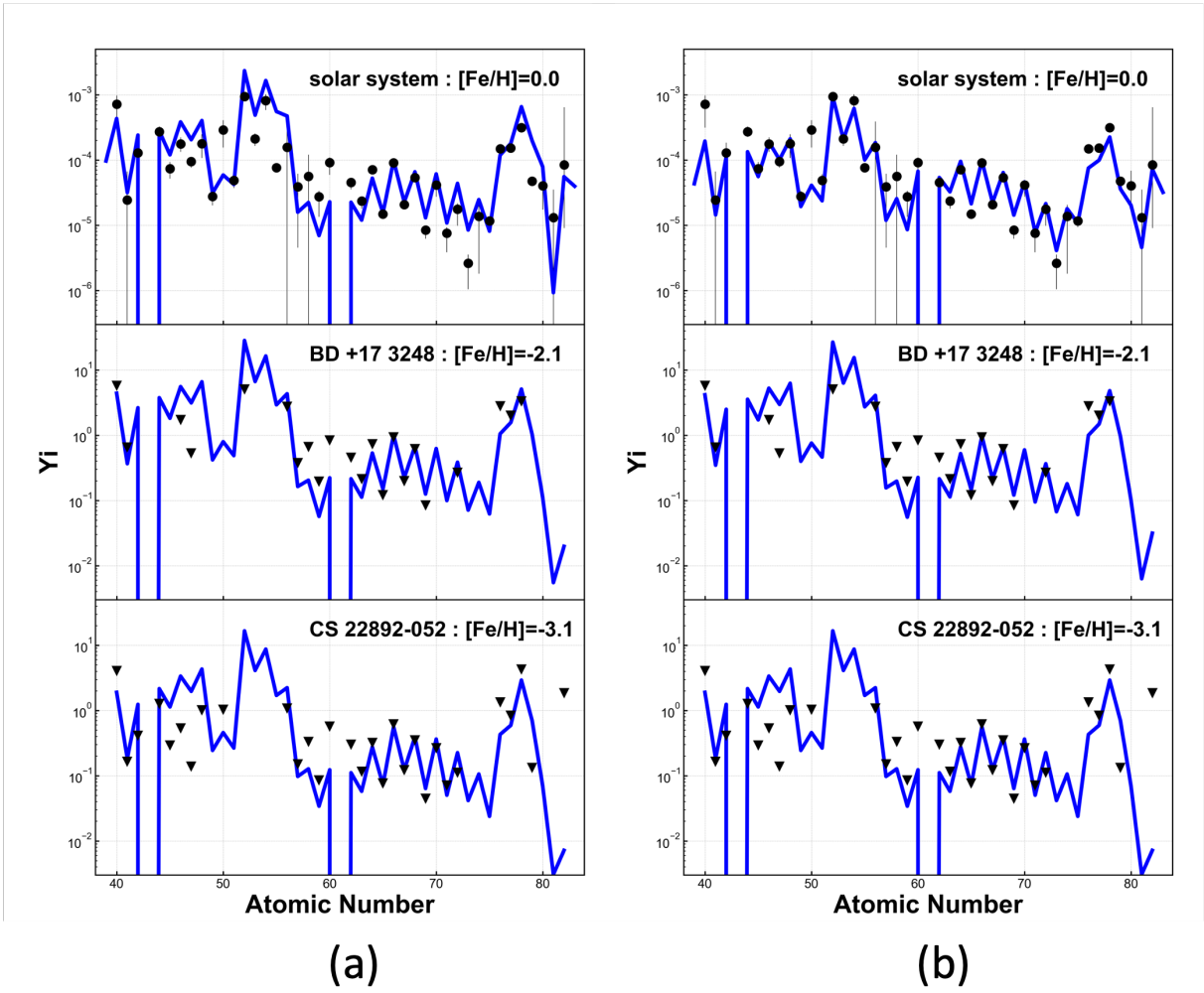

Fig. 20. The elemental abundance pattern in the case of Model 2-s and Model 2-a. The updated version of Fig. 3 in Yamazaki et al. (2022) [39]

nucleosynthesis calculations, and associated input nuclear physics, FFD.

Although the elemental abundances are in reasonable agreement with observational data, there are some exceptional elements, to be discussed below, which show discrepancy with observations.

One finds a discrepancy for lighter elements Zr-Sn (Z=40-50) in CS 22892-052. A significant enhancement of these elements has been reported in the so-called Honda stars [2]. Our present theoretical interpretation is that the universality between the second and third peaks including the lanthanide hill around $Z \approx 66$ and beyond is satisfied in any cases, although the variation in a wider mass range can be reasonably explained by inhomogenity in the early galaxy.

As for the second and third peak nuclei around $Z \sim 52$ and 78, strong model dependence arises from different contribution fractions of NDW, MHDJ and NSM in *Model 1* and those of NDW, collapsar and NSM in *Model 2*, as discussed in Figure 20. Only Te (Z=52) among nuclei which form the second r-process abundance peak was observed by using spectrograph equipped on HST [40].

Interestingly, the actinides are also significantly enhanced in the collapsar r-process. This is because the extremely high neutron number density in collapsars causes the r-process path to proceed along very neutron-rich nuclei and produce neutron-rich isotopes beyond the third peak. Such a dramatic enhancement of actinides is indeed observed in actinide-boost stars [42].

Many features of elemental abundance patterns are more or less similar to one another among Models 1 and 2 with either symmetric or asymmetric FFDs being used.

4.2 The evolutional track in the [X/Fe]-[Fe/H] plane

One of the most important factors in metallicity changes in heavy-element composition is the contribution from the s-process as well as the r-process. Studies of solar composition at [Fe/H]=0 suggest that more than 90% of strontium was produced by the s-process. On the other hand, more than 90% of the europium in the solar system is thought to have been produced by the r-process. We therefore investigated strontium and europium as typical elements formed mainly by the s- and r- processes, respectively.

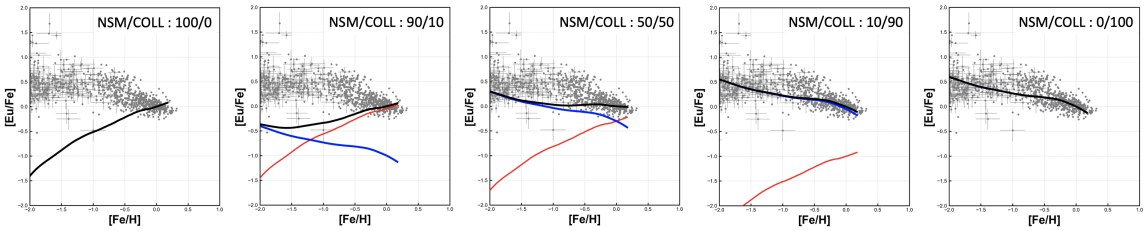

Fig. 21. Illustration of [Eu/Fe] as a function of metallicity [Fe/H] for different relative contributions of callapsars and NSMs as described in the text. Black lines show the total abundance. The blue lines are the collapsar contribution while the red lines show the contribution from NSMs. Grey dots show the data from metal-poor halo stars. The minimum coalescence time for NSMs is taken to be $\tau_g = 10$Myr. Reprinted from Fig.4 in Yamazaki et al. 2022 [39]

The r-process component in the metal abundance change of the heavy element composition depends on the extent to which each r-process site contributes. The contribution of each r-process site depends on the element and also on the choice of nucleosynthesis calculations and nuclear physics, which still have large theoretical uncertainties. Therefore, we surveyed the relative contribution of each r-process site when artificially varied. For the sake of simplicity, we only consider the contributions of NSM contributions only. Only the contributions of collapsar and NSM are listed, since similar results can be obtained by considering CCSNe

Figure 21 shows the evolution of the [Eu/Fe] ratio as a function of metallicity. The contribution fractions from NSMs are 100%, 90%, 50%, 10%, 0% from left to

right. The contribution from collaspars is opposite. If less than 50% of europium is produced by NSMs, the evolution curve at [Fe/H]> -1 becomes flat as discussed in [24]. Although the contribution fraction of NSMs somewhat depends on the choice of the minimum coalescence times τ_g =1,10 and 100 Myr for binary NSMs, the flattening of the curve at [Fe/H]> -1 is independent of the choice of τ_g.

As can be seen from Figures 17 and 18, in the presence of NSM dynamical ejecta with asymmetric FFD, the solar system's europium abundance is dominated by the NSM. Since this is not consistent with the europium distribution of the galactic halo, we expect a small fraction of the contribution from the dynamical ejecta component of the NSM.

On the other hand, it is very difficult to separate the collapsar and CCSNe contributions in such a schematic analysis. This is because the difference between the two components is found in the super metal-poor region, where the non-uniformity is pronounced.

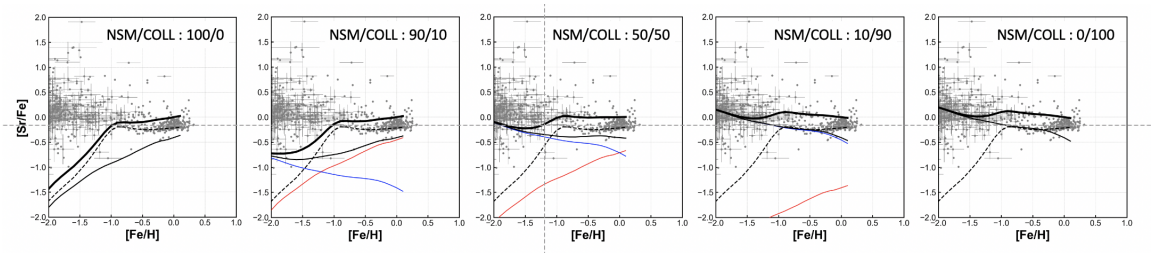

Fig. 22. Illustration of [Sr/Fe] as a function of the metallicity [Fe/H] for different relative contributions of collapsars and NSMs Both r-process (solid) and s-process (dashed) contributions are shown. Black lines show the total abundance. The blue lines are the collapsar contribution while the red lines show the contribution from NSMs. Grey dots show the observed abundances on metal-poor halo stars. The minimum coalescence time for NSMs is taken to be $\tau_g = 10$Myr. Reprinted from Fig.5 in Yamazaki et al. 2022 [39]

Figure 22 shows the variation of the [Sr/Fe] abundance ratio versus metallicity. s-process contributions are taken from Kobayashi et al. (2004 kobayashi2004. The analysis of the [Sr/Fe] distribution supports the small contribution of NSM here as well. This fact justify our model configuration that we do not include the disk wind

component of NSM which mainly produce the light r-process elements such as Sr. However, this alone does not distinguish which theoretical model represents the true contribution. Therefore, it is desirable to compare theoretical models with future observations to determine which astrophysical positions an element is derived from.

4.3 Conclusion

In summary, we have studied the cosmic evolution of r-process abundance patterns in the context of a GCE model that simultaneously takes into account multiple astrophysical sites, namely NDW and MHDJ CCSNe, NSM and collapsers. NSM r-process calculations were performed using a variety of input nuclear physics, including symmetric and asymmetric FFD. Second, while the early galaxy r-process component is dominated by yields from CCSNe and collapsers, the NSM contribution is necessarily delayed due to the cosmologically long coalescence timescale of orbital collapse by emitting GW. The relative NSM contribution increases rapidly with cosmic time. However, it does not reach even 1% of the total solar r-process composition until the metallicity is enriched to [Fe/H]$\geq$ -1.5. This conclusion does not change for a wide range of minimum coalescence times of τ_g = 1 - 100 My for any GCE model with multiple sites and different input nuclear physics.

We also find that there are large differences in isotopic abundance patterns as a function of mass number among multisite GCE model calculations, but the universality of elemental abundances in metal-poor halo stars is still satisfied. This contrasts with previous studies that focused only on single r-process sites or combinations of up to two astrophysical sites to explain the universality of elemental abundance patterns.

Some unique features of each astrophysical site are still expected in the GCE of isotopic mass A abundance patterns. Notably, the collapsar contribution is dominant from the beginning of early galaxies. Also, in both collapsars and NSMs, the abundance peaks shift towards the heavier mass regions due to the high residual neutron flux during the freezeout of the r process.

Elemental Z abundance patterns are more or less similar between models, but exceptional differences can be found in actinide or light r-process elements, especially at Z<42. So these are important indicators. of the dominant r-process site. Also, the peak structure is model dependent due to the different contributions from the four astrophysical sites considered here.

Therefore, it is highly desirable to continue spectroscopic observations with next-

generation telescopes such as the 30-meter telescope. They will provide metal abundance dependence and abundance peaks of isotope abundance ratios for actinides, lanthanides, and lighter elements. The isotopic separation of each r-process element may constrain the evolution of NSMs, MHDJs and collapsers beyond the evolution of models with a single r-process site.

5 Introduction and Our Method of p-nuclei and νp-process

5.1 Introduction of νp-process studies

The p-nuclei are stable nuclides with atomic numbers Z $\geq$ 34 that are located on the proton-rich side of the β-stability line [43]. The isotopic fractions of the p-nuclei are typically lower than 1.5%. Such p-nuclei are not synthesized through the r- or s-process that predominantly contributes to production of heavy nuclei. It was suggested that the p-nuclei may be produced by (p, γ) and (γ, p) reactions [43]. Woosley and Howard (1978) [44] and Hayakawa et al. (2004) [45] have provided evidence confirming that most p-nuclei are synthesized by successive photodisintegration reactions from heavier isotopes in high temperature environments (γ-process).

Candidates for the γ-process astrophysical sites include O-Ne rich layers in CC-SNe [44, 46, 47, 48, 49] and the outermost layers of exploding carbon-oxygen white dwarfs; SNe Ia [50, 51, 52, 53].

Calculations of γ-process nucleosynthesis could produce the abundances of most p-nuclei except for ^{92,94}Mo and ^{96,98}Ru. The solar isotopic fractions of these four nuclei are 14.84, 9.25, 5.54, and 1.87%, respectively. These fractions are much higher than those of other p-nuclei. The large isotopic fractions imply another astrophysical process for the origin of these four nuclei which produce non-negligible amount of nuclei.

Howard et al. (1991) [50] showed the nucleosynthesis in SNe Ia to describe the abundance of Mo and Ru isotopes in a combination of photolysis and particle-induced reactions.

However, GCE simulations by considering SNe Ia [54] and SNe II [55] could not sufficiently produce the abundance of Mo and Ru p-isotopes at the solar metallicity.

Frohlich et al. (2006) [56] proposed a new mechanism of nucleosynthesis by the νp-process. This process takes place in the proton-rich neutrino-driven wind (NDW) of SNe II via free neutrons produced when electron antineutrinos are absorbed by free protons, i.e. $p(\bar{\nu}_e,\ e^+)n$. This increases the abundance of ^{92,94}Mo and ^{96,98}Ru. A large amount of p-nuclei are produced through νp-processes [56, 57, 58], a series of $(n,\ p)$ and $(p,\ \gamma)$ reactions. Uncertainties in the νp-process, such as the hydrodynamic state variables of the NDW, neutrino flux, and nuclear reaction rate, have been widely studied [59, 60, 61, 62, 63, 64, 65, 66].

Nevertheless, there has been little clear observational evidence that these proposed processes actually occurred in the Galaxy, such as solar-matter abundances, in particular isotopic anomalies in primordial meteorites, and stellar chemical compositions.

It has been recently reported that the abundance ratios observed in the Cassiopeia A supernova remnant are the result of α-rich freeze-out and proton-rich ejecta [67] from neutrino process. In addition, molybdenum isotopic anomalies in both differentiated (i.e., melted asteroids) and primitive meteorites (i.e., carbonaceous chondrites) have been reported [68, 69, 70]. In particular, the enhancement of isotopic anomalies in p-isotope ^{92,94}Mo was found to correlate with that of r-isotope ^{100}Mo [68, 69]. On the other hand, isotopic abundances observed in iron meteorites [70] show a different pattern, in which the ^{92}Mo anomaly is only weakly correlated with the ^{100}Mo anomaly. These results indicate that ^{92,94}Mo may have been synthesized by a different nucleosynthetic process in the same star that produced ^{100}Mo.

The νp-process in core-collapse SNe, where the r-process also occurs, is one of the candidate sites for the production of ^{92,94}Mo and ^{96,98}Ru. Observational evidence that these four nuclei are predominantly synthesized in the νp-process may be found in metal-poor stars with reported elemental compositions of Mo and Ru.

In this thesis, we study the GCE of Mo and Ru. First, we determine yield data for νp-processes in various SN models. Since these processes depend on the hydrody-

namic states of the NDW in SNe II, we consider different hydrodybamic models. In particular, we evaluate the yields of $^{92,94}Mo$ and $^{96,98}Ru$ in the νp-process based on simulations of SNe II and a higher energy SN event ($\sim 10^{52}$ erg). We then apply these four anomalous p-nucleus yields to the GCE and analyze the various contributions to the solar composition from the νp-process.

We show that the produced amount of the νp-process in hypernovae could explain the enhanced elemental abundances of Mo and Ru observed in metal-poor stars.

We note that complementary GCE studies for Mo and Ru (including Sr, Y, Zr, and Ba) have recently been reported in Vincenzo et al. (2021) [71]. In that study, they similarly concluded that the production of Mo and Ru in the NDWs ejected from protoneutron star (PNS) in SNe is insufficient to explain the observed abundances of Mo and Ru at low metallicity unless arbitrarily enhanced by a factor of about 30. They therefore considered that the effect of a fast-rotating PNS might provide the required rate of intensification (although these models predict larger [Sr/Fe] and [Mo/Fe] at higher metallicities). This study differs in that it employs standard production factors and demonstrates that the additional production at lower metallicity is due to the contribution from the νp-process from HNe.

5.2 Hypernova νp-process

We estimated the abundance of p-nuclei produced by νp-processes in both SNe II and HNe; in the case of SNe II, the entropy per baryon is small in the early stages of the explosion ($t < 1$ s) and the long timescale associated with the initial dynamic ejection [72] p-nucleation due to νp-processes is small. Therefore, we focus on νp-processes in the late stages of the explosion ($t > 1$s). We construct models of general relativistic steady-state spherically symmetric NDWs by using the method described in Otsuki et al. (2020) [73] for various electron fractions Y_e, neutrino luminosities L_ν, neutrino average energies E_ν, PNS radius R_ν and PNS gravitational mass $M_{\rm PNS}$. The hydrodynamic quantities associated with wind trajectories in each different progenitor model are calibrated with numerical results for $9, 12, 25$ and 60 $M_\odot$ models obtained in recent 3D core-collpase SN simulations [74, 75].

The existing 3D explosion model hydrodynamic simulations stop at ~ 1 seconds. We extrapolate them to subsequent times as follows $L_\nu(t) = L_{\nu,0}\exp(-(t-t_0)/\tau_\nu)$, as used in Woosley et al. (1990) [76], where the neutrino luminosity decreases exponentially when the fluid simulation stops at $t = t_0$. The time after this is estimated as where $L_{\nu,0}$ is the neutrino luminosity at $t = t_0$ and $\tau_\nu = 1$ s is the timescale of neutrino cooling. Here, $L_{\nu,0}$ is the neutrino luminosity at $t = t_0$ and $\tau_\nu(= 1$ s) is the timescale of the neutrino cooling. The values of t_0 for different models are given in Table 2 in Burrows et al. (2020) [74]. The change in the radius of the PNS is $R_\nu(L_\nu) = (R_0 - R_1)(L_\nu/L_{\nu,0}) + R_1$ [6], where R_0 is the PNS radius at $t = t_0$ and R_1 is the radius of the PNS after cooling, which sets equal to R_1=12 km to satisfy the observational constraints on the typical radius of cold neutron stars.

Furthermore, we consider that the neutrino temperature decreases as the neutrino cooling proceeds. Assuming that neutrinos follow a Fermi-Dirac distribution with no chemical potential, the neutrino temperature $T_\nu = \langle E_\nu\rangle/3.151$ is proportional to $(L_\nu R_\nu^{-2})^{1/4}$ when $t > t_0$. This relation reveals that T_ν decreases as L_ν decreases. The numerical settings of the network simulation are the same as those in [62]. In this model, the energy spectra of different neutrino species are nearly degenerate in the

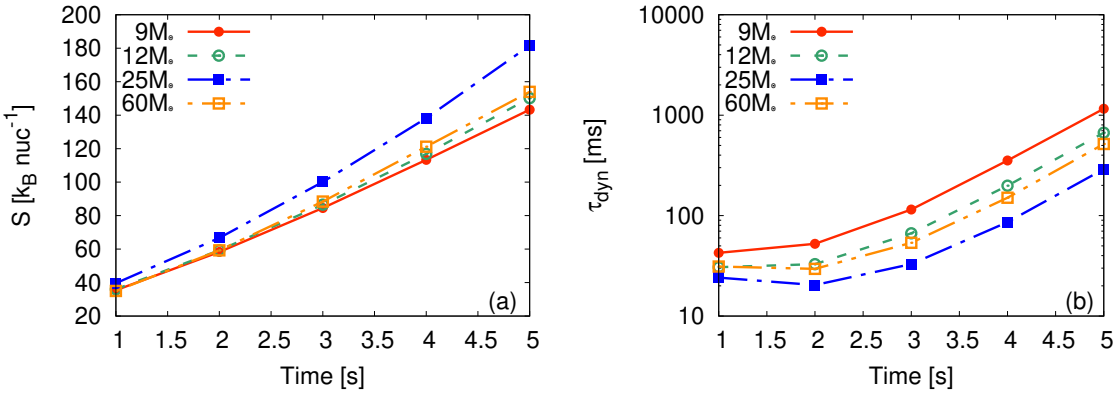

late stage of the explosion ($t > 1$ s), so the effect of neutrino oscillations is neglected. The total yield of nucleus i inside the NDW is $y_i = \int_{t=1\mathrm{s}} \mathrm{d}t\ X_i(t)\dot{M}(t)$ where $\dot{M}(t)$ is the mass ejection rate inside the wind orbit and $X_i(t)$ the nuclear mass fraction at time t. The total yields of p-nuclei in the NDW models with initial masses $9, 12, 25$ and 60 $M_\odot$ are used as input data for the subsequent GCE calculation.

The νp-process in the HN model is based upon NDWs obtained in [61] where the possible synthesis of heavy elements in a 100 $M_\odot$ progenitor star was investigated. In this progenitor model, a massive PNS ($\sim 3M_\odot$) is maintained for a few seconds before a black hole forms. We adopt the NDW model (e) in Table 3 of [61] as the fiducial model of proton-rich NDWs in HNe. The yield of p-nuclei is obtained by multiplying a typical lifetime of massive PNSs ($\tau_{NS} \approx 1$ s) by the mass ejection rate ($\dot{M}$) and the mass fraction (X_i) of the p-nucleus in the trajectory of model (e).

The νp-process is sensitive to the hydrodynamic quantities of the NDW. Figure 23 shows the time evolution of various hydrodynamic quantities for the NDW in our SN II model, including entropy S per baryon, extended timescale τ_{dyn}, electron fraction Y_e and mass ejection rate $\dot{M}(t)$. Here we show the values of entropy and expansion timescales at high temperatures ($T = 0.5$ MeV) before nucleosynthesis of heavy elements as in [73]. The mass of the PNS in our SN II model is shown in Table 2. S (τ_{dyn}) is higher (lower) at each explosion time as the mass of the PNS becomes larger. Both S and τ_{dyn} increase with the explosion time. Such hydrodynamic properties of S and τ_{dyn} are consistent with the results of Otsuki et al. (2000) [73] and Wanajo

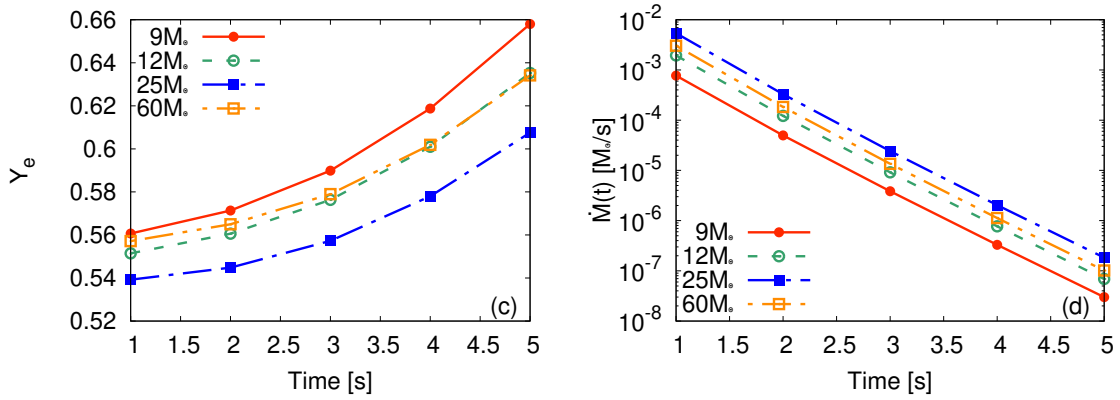

Fig. 23. Time evolution of hydrodynamic quantities associated with NDWs. (a) entropy per baryon, (b) expansion timescale, (c) electron fraction, and (d) mass release rate in different SN II progenitors. Reprinted from Sasaki et al, 2022

(2013) [6], even though they studied r-process nucleosynthesis in NDWs with a neutron excess ($Y_e < 0.5$). Nucleosynthesis inside the NDW is sensitive to the electron fraction. The electron fraction at the beginning of the network simulation ($T = 10^{10}$ K) is shown in Figure 23(c). The NDW is proton-rich ($Y_e > 0.5$), and the νp-process occurs in our wind model: the difference between$\langle E_{\bar{\nu}_e}\rangle - \langle E_{\nu_e}\rangle$ gets smaller as the explosion time passes, so the value of Y_e becomes large and almost independent of the primordial models. Figure 23(d) shows that the wind mass ejection rate $\dot{M}(t)$ becomes smaller with decreasing neutrino luminosity and that the contribution of the late phase ($t > 5$ s) to the total p-nuclear yield is negligible in our wind model.

Type	Progenitor Mass	PNS Mass	^{92}Mo	^{94}Mo	^{96}Ru	^{98}Ru
SN II	9	1.2	1.1×10^{-15}	1.4×10^{-16}	2.5×10^{-17}	2.4×10^{-18}
SN II	12	1.4	1.6×10^{-14}	2.0×10^{-15}	4.0×10^{-16}	3.6×10^{-17}
SN II	25	1.7	8.2×10^{-12}	1.8×10^{-12}	4.9×10^{-13}	7.7×10^{-14}
SN II	60	1.5	4.4×10^{-13}	6.7×10^{-14}	1.4×10^{-14}	1.5×10^{-15}
HN	100	3	2.0×10^{-7}	1.5×10^{-7}	1.6×10^{-7}	2.9×10^{-7}

Table 2. PNS masses and yields of the p-nuclei in the νp-process of different progenitor models (in $M_\odot$). (Reprinted from Sasaki et al, 2022)

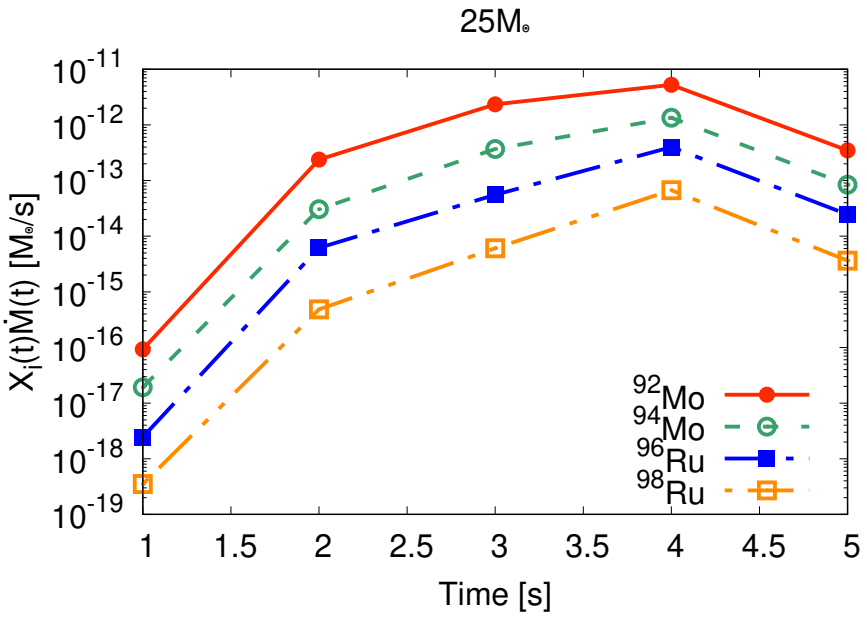

Fig. 24. Time evolution of the p-nuclear yields in the νp-process of the $25M_\odot$ SN model. Reprinted from Sasaki et al, 2022

Figure 24 shows the production rate of p-nuclei by the νp-process in the NDW at different times during the SNe II explosion. This figure shows the time evolution of the yields of ^{92,94}Mo and ^{96,98}Ru produced by the νp-process in the $25M_\odot$ SNe II model. The total yield y_i is given by the time integral of $X_i(t)\dot{M}(t)$ as defined above.

The other $9M_\odot$, $12M_\odot$, and $60M_\odot$ models also have different values of y_i depending on the model, but the general trend is the same. The νp-process is a primary process that proceeds without a pre-existing seed core derived from an earlier generation star. A seed nucleus heavier than helium is synthesized in the initial stage before the νp-process, and nucleosynthesis proceeds from this seed nucleus through reactions with light particles such as protons and α particles.

The production yield of the νp-process depends on the ratio of the number of free neutrons produced via $p(\bar{\nu}_e, e^+)n$ to the number of seed nuclei, denoted by Δ_n [64]. Heavier p-nuclei are synthesized with higher Δ_n. The value of Δ_n in the wind trajectory of the SN II model for $25M_\odot$ is smaller than 10, therefore around the mass

number $A \sim 100 - 110$, νp-process does not produce heavy nuclei efficiently. Therefore, the p-nuclei yields shown in the figure are larger than the yields of p-nuclei heavier than $A = 100$ at any explosion time. The yield of each p-nuclei increases up to $t = 4$ seconds, because the entropy per baryon S also increases as the neutrino luminosity decreases (see Figure 23(a)). This production of heavier p-nuclei in wind with higher entropy has been also confirmed in previous studies [59, 64].

On the other hand, if the neutrino luminosity at $t > 4$s is small, the production of p-nuclei is suppressed. This is because the expansion time scale of the wind orbitals increases at $t > 4$ seconds, and a large number of seed nuclei are produced to produce heavy elements, resulting in a smaller value of Δ_n (see, for example, equation (9) in Xilong et al. (2020) [65]). The contribution from the late explosion phase ($t > 5$ seconds) is negligible in the current SNe II model because the mass ejection rate of each wind orbit continues to decrease.

The table shows the masses and yields of ^{92,94}Mo and ^{96,98}Ru, when 9, 12, 25 and 60 $M_\odot$ models correspond to SNe II and 100 $M_\odot$ models correspond to HNe. p-nuclei yields are sensitive to PNS mass. In the case of massive PNSs, the entropy per baryon of the wind trajectories becomes large and, in contrast, the expansion time scales become short [73, 59, 6] because of general relativistic effects. Both conditions of the higher entropy and the shorter expansion time scale result in a higher value of Δ_n and a larger production of heavy p-nuclei in progenitor models having a more massive PNS. The yields of p-nuclei in the HN model is much larger than those in the SNe II models because the PNS mass of the HN model ($M_{\rm PNS} = 3M_\odot$) is much heavier than those of the SNe II models ($M_{\rm PNS} < 2M_\odot$). This implies that the νp-process in HNe can play an important role in the GCE of Mo and Ru.

The yield of p-nuclei produced by the νp-process in SNe II is much smaller than that in HNe. However, we point out that the effects of inverse shocks and fast neutrino flavor conversion [65] may increase the p-nuclei yield. We discuss these uncertainties in the νp-process again in Chapter 6.3.

6 The Calculated Results of νp-process GCE

6.1 Impact of νp-process on the p-nuclei evolution.

6.1.1 Mass distribution of p-isotopes at the present metallicity

We have performed GCE calculations that include contributions from the νp-process and various other nucleosynthesis processes. As a result, the relative contributions of νp-processes to the abundances of ^{92,94}Mo and ^{96,98}Ru in the solar system and stars are analyzed. There are seven stable isotopes of Mo. Of these, ^{92}Mo and ^{94}Mo are p-nuclei, and ^{96}Mo is only an s-nucleus because it is shielded from $\beta^{\pm}$ decay by the stable isotopes ^{96}Ru and ^{96}Zr. The other isotopes are produced by s- and r-processes; the nucleosynthetic origin of Ru is similar to that of Mo: ^{96}Ru and ^{98}Ru are p-nuclei, ^{100}Ru is an s-only isotope, while the other Ru isotopes are synthesized by both s- and r- processes.

The framework for GCE calculations for p-nuclei is based on the one-zone model of Timmes et al. (1995) [19] and Yamazaki et al. (2022) [39]. This model includes an exponentially decaying galactic inflow and a star formation rate calculated using the second-order Schmidt function [77].

Except for the p-nucleus, the evolution of the s and r nuclei with respect to metallicity is taken from Kobayashi et al. (2020) [23] and Yamazaki et al. (2022) [39], respectively. The GCE model used in Kobayashi et al. (2020)[23] is different from ours, but the GCE of the s-nucleus is identical to ours. The GCE of the s-process is almost independent of the model employed and is rather robust, compared to the r-process. In addition, the s process is a secondary process and its progenitors are long-lived low- and intermediate-mass stars, which do not contribute significantly to the GCE.

The production rate of each p-nucleus is derived from the event rate of SNe, including HNe, and the ejected mass of the synthesized p-nucleus associated with each progenitor. The mass range of HNe is constrained following the initial mass function (IMF) of Kroupa [22]. The mass ranges of the SNe and HNe at zero-age main-sequence are assumed to be $8-60\ M_{\odot}$ and $60-100\ M_{\odot}$, respectively. In this

configuration, 4% of the massive stars explode as HNe, and this fraction is consistent with the value recently deduced in Shivvers et al. (2017) [78]. The delay time τ for the SN (or HN) explosion of a massive star due to stellar evolution is set to be equal to the main-sequence lifetime as a function of ZAMS mass.

Table 2 summarizes the input data taken from Fujibayashi et al. (2015) [61] for the νp-process yields that we used in our GCE model calculations. Although some variation in the νp-process depending on the PNS mass and metallicity of HNe is expected, it is beyond the scope of the present study because the primary purpose of this study is to identify the contribution from HN νp-process to the production of p-nuclei, in particular of ^{92,94}Mo and ^{96,98}Ru whose solar isotopic fractions are one order of magnitude larger than those of the other p-nuclei.

As for the γ-process, both SNe Ia and SNe II contribute to the solar composition of p-nuclei, as pointed out by Travaglio et al. (2015) [54]. There is much debate about the γ-process yields. The reader should know that the γ-process yields in this thesis were obtained from calculations by Kusakabe et al. (2011) [52] for SNe Ia and Travaglio et al. (2018) [55] for SNe II, respectively. In our GCE calculations, we used the p-nucleus yields of Kusakabe et al. (2011) in case A1 to account for the contribution from SNe Ia. Another contribution from γ-process in SNe II was taken from the model calculation that does not include the contribution of nucleosynthesis inside the NDW (*xi45* KEPLER model) [55]. These models cover the initial progenitor masses from $M = 13M_{\odot}$ to $30M_{\odot}$ and metal mass fractions from $Z = 0$ to 3.1×10^{-2}.

Note that the γ-process in SNe II occurs by photodisintegration in the O-Ne-Mg outer layer at regions with radii $\gtrsim$10000 km. On the other hand, the νp-process occurs inside the NDW near the PNS atmosphere at $\sim$100 km. Thus, it is clear that the νp-process contribution in the NDW is not included at all in the *xi45* KEPLER model. The KEPLER model is based on SNe II at different primordial masses and metallicities. It provides the nuclear yields of p-nuclei produced by the γ-process.

Figure 25(a) shows the final mass fractions of p-nuclei (circles) in the solar metallicity obtained from GCE calculations. They are compared with the solar composition (squares). The upper and lower triangles correspond to the γ-process of SNe II only

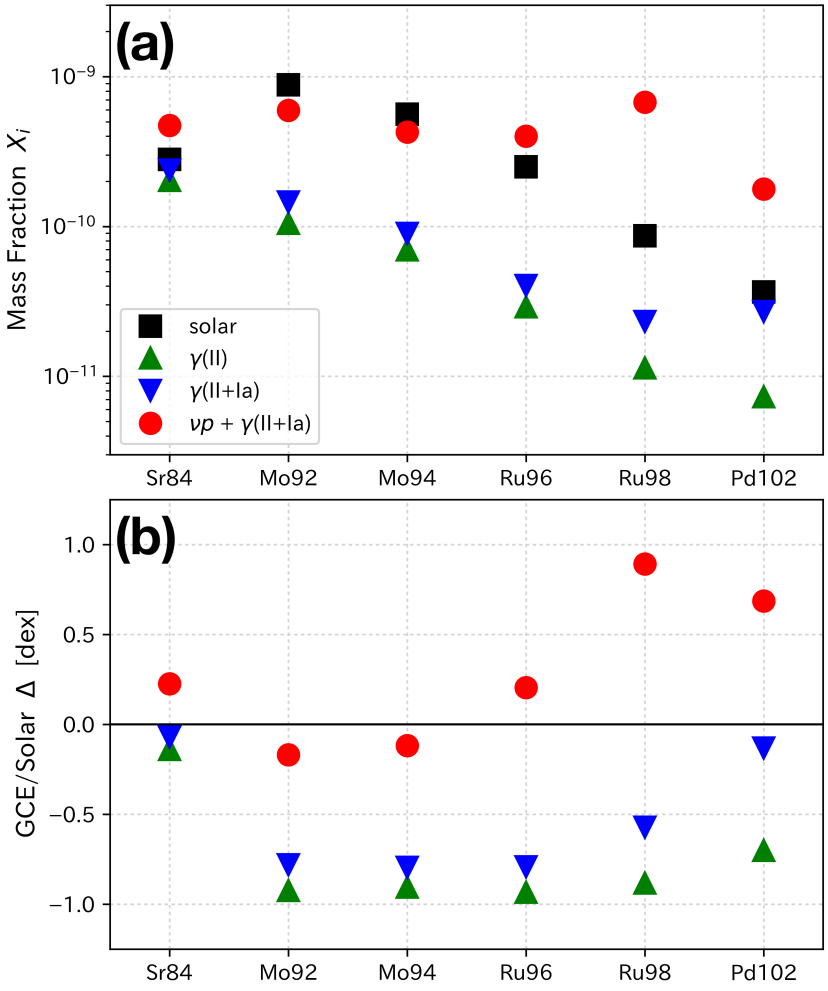

Fig. 25. Final abundances of the p-nuclei at [Fe/H]=0 compared with the solar system abundances. Reprinted from Sasaki et al, 2022

or the combined contribution of SNe II and Ia, respectively. The red circles correspond to the total yield of the νp-and γ-processes. Figure 25(b) shows the ratio of theoretical to observed solar abundances in a logarithmic scale, indicating that the solar abundances of ^{92,94}Mo and ^{96,98}Ru are underestimated by the contribution from the SNe γ-process alone, and the contribution from SNe Ia is insignificant. On the other hand, νp-processes significantly increase the theoretical abundances of these p-nuclei. The νp-process contribution in the figure comes mainly from HNe, as shown in Table 2. This influence of νp-process in SN II is consistent with the discussion of Xilong et al. (2020) [65] and Jin et al. (2020) [66] in the absence of inverse shocks and fast flavor conversion of neutrinos. HN (or SN) progenitors with massive PNS enhance the contribution of the νp-process to the solar system composition of the p-nucleus.

The overproduction of ^{98}Ru and ^{102}Pd would require some modification of HN models although the predominance of HN νp-process among many other processes might not change in the production of these abundant p-isotopes. Another solution to this overproduction could be an effect of nuclear physics: The yields of heavier p-isotopes might be suppressed if recently proposed large triple α reaction rate [66] is used in the network calculation. Newly proposed four-body reaction mechanism is expected to enhance the triple α reaction rate [66], which results in increasing seed abundances of Fe-Ni-Zn and decreasing heavier p-isotopes. This is because the free neutrons produced in the νp-process are exhausted by the abundant seed nuclei before the reaction flow reaches the production of heavier p-isotopes ^{98}Ru and ^{102}Pd.

6.1.2 The Evolutionary track in the [X/Fe]-[Fe/H] plane

Figure 26 shows the relationship between the element ratio [X/Fe] and [Fe/H]. The filled circles are the observed data of stars obtained from the SAGA database [79]. The black dotted and dashed lines represent the r- and s-process compositions, respectively. The thin dashed line in Figure 26(a) shows the total abundance of p-isotopes ([(^{92}Mo+^{94}Mo)/Fe]) of SNe excluding the γ and νp-processes of HNe. The thin solid line (red) shows the abundance ratios of Mo p-isotopes produced from the γ process, the SN νp-process, and the HNe νp-process. The thick red solid and thick blue dashed lines show the total element abundances in the GCE model calculations with and without the contribution of the HNe νp-process, respectively. The blue dashed lines show that the γ- and νp-processes from SNe alone do not explain much of the evolution of the Mo abundance ratio in the total metal abundance region. In the [Fe/H] $<$ -1 region, the contribution of s-processes is also negligible.

On the other hand, the r-process (dotted line) makes a relatively large contribution in the [Fe/H] $<$ -1, but the r-nucleus abundance is somewhat less than the observed stellar abundance. As shown in the red thick and thin solid lines, the νp-process in HNe significantly enhances the abundance of p-isotopes, and the production by the HN νp-process is larger than that by the r process in the [Fe/H] $<$-2 region. Therefore, it can be seen that HNe are the dominant contributor to the νp-process at [Fe/H]< -2. This result indicates that the Mo abundances observed in the low metallicity region are mainly produced by the νp-process of HNe. Since the early Galactic population III stars are considered to have a high mass of $\sim 100 M_{\odot}$, the conclusion that HNe are dominant in the low-metallicity region seems reasonable.

Figure 26(b) similarly shows the elemental abundance of Ru with and without the νp-process in HNe. It can be seen that the γ- and νp-processes of SNe II have little effect on the elemental abundance of Ru, while the νp-process of HNe increases the elemental abundance in the low metallicity region. The contribution of the HN νp-process to the Ru elemental abundance is not as pronounced as that of Mo. This is because the isotopic ratio of ^{92,94}Mo is as high as 24.1%, while Ru (^{96,98}Ru) is as

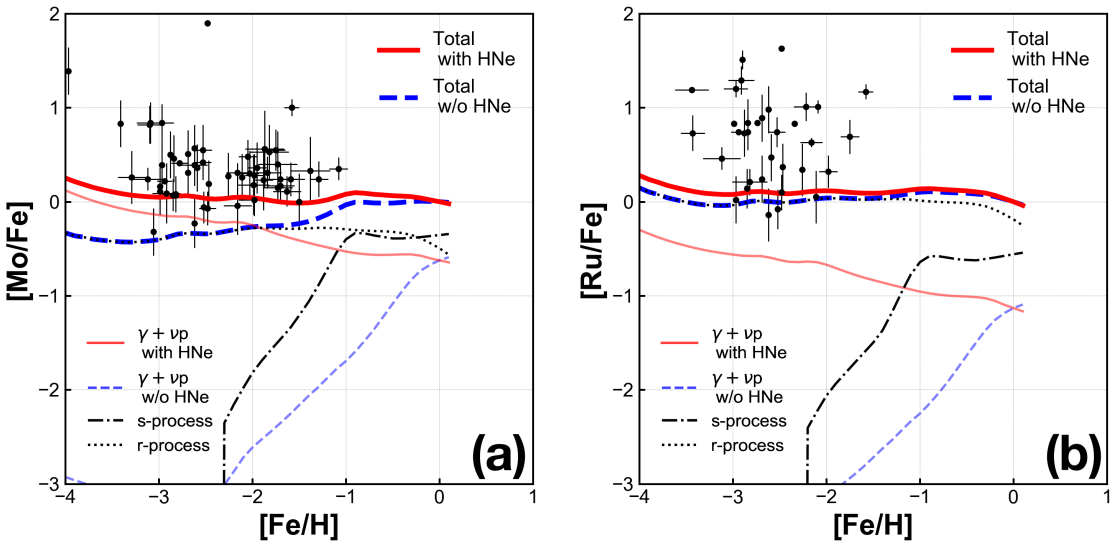

Fig. 26. Elemental abundance evolution of (a)Mo and (b)Ru. Thin lines show each process contribution. Thick lines are the total elemental abundances. Solid lines include the contribution of the νp-process in HNe while the dashed lines do not. Reprinted from Sasaki et al, 2022

low as 7.4%, so the contribution of νp-processes is not as pronounced as Mo We note that ^{92,94}Mo may be synthesized even in slightly neutron-rich emissions ($Y_e \sim 0.47$) [63, 72]. If the initial neutron excess ejecta of CCSNe with $t < 1$s is taken into account in the GCE calculations, the total amount of Mo and Ru may increase and the theoretical predictions may be more consistent with the observed abundances.

Figure 27 shows how our GCE model describes the evolution of other elements. The figure illustrates the mass ratios of [Sr/Fe] and [Pd/Fe] to [Fe/H]. These two elements were chosen because their abundances in the solar system are known to be dominated by the s and r process contributions [80]. In these nuclei, the pure p-process isotopes are limited to ^{84}Sr (isotopic ratio of 0.56%) and ^{102}Pd (1.02%).

The νp-process contribution of HNe increases with decreasing metal content (thin red solid curve), as do for Mo and Ru in Figure 27. However, unlike the GCE for Mo and Ru, Sr and Pd show that the s+r component is dominant in the metallicity region of $-4 <$ [Fe/H] < 0. In addition, the νp- and γ-process contributions are

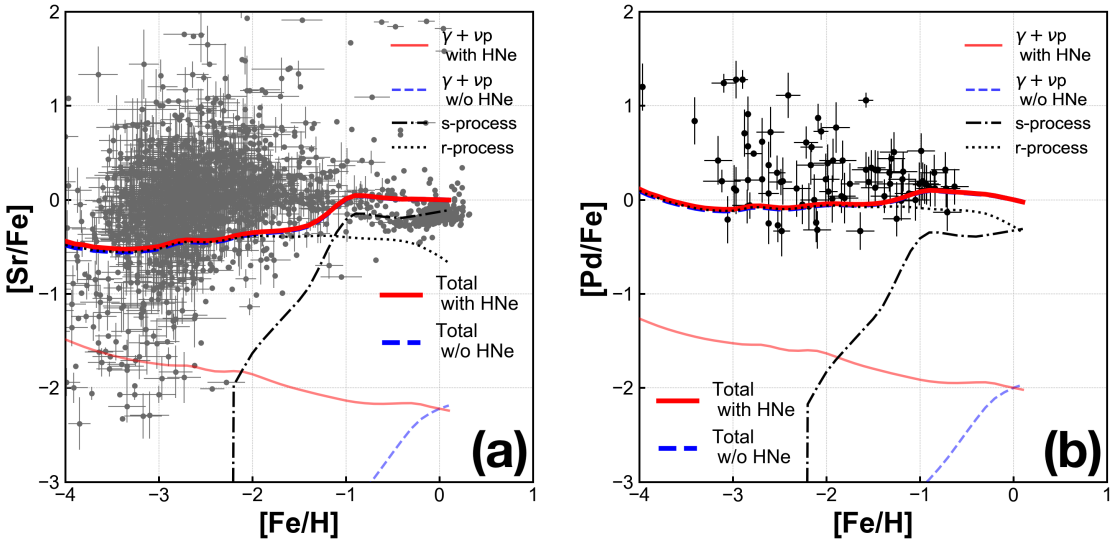

Fig. 27. Elemental abundance evolution of (a) Sr and (b) Pd as in Figure 26. Reprinted from Sasaki et al, 2022

less than 1% even at [Fe/H] = −4, both with and without contributions from HNe. Therefore, we emphasize that Mo and Ru are particularly important in GCE studies because of their large fraction of pure p-isotopes.

Our GCE model provides abundance curves through the bottom of the observed abundance distribution of the elements in Figures 26 and 27. The observed variation in elemental composition is mainly due to the non-uniformity of SN and HN emissions, including explosive nucleosynthesis products [81, 82]. In our GCE model without taking account of non-uniformity, the SN and HN emissions are uniform during the metal-poor GCE epoch. This is true for all four abundance distributions of Mo, Ru, Sr, and Pd elements.

However, the GCE of the νp-process elements may depend more or less on various quantities, such as the initial mass of the primordial star, metal abundances, SN and HN event rates, etc. It is very difficult to take all these quantities into account. Although we here have assumed that the sensitivity to the initial mass of the HNe is weak, the sensitivity to the primordial mass range is examined quantitatively. We

estimate the sensitivity of HNe to the primordial mass range of HNe in the three cases $60 - 120M_{\odot}$, $60 - 100M_{\odot}$, and $40 - 100M_{\odot}$, while keeping the nucleosynthesis yield of HNe the same. We then find that the [X/Fe] difference is less than 0.2, and that this is only noticeable in the low metallicity region with [Fe/H] < -2.5. Thus, we can conclude that the GCE result is not very sensitive to the HNe primordial mass range.

As discussed previously, the enhanced isotopic abundance of ^{92,94}Mo is correlated with the enhanced isotopic abundance of ^{100}Mo in primitive meteorites [68, 69, 70]. Core-collapse SNe are still strong candidates for the astrophysical site of the r process. If a single SN occurred near the protosolar nebula and both the νp- and r-processes occurred in that SN, the products would have contaminated the protosolar material as observed in protometeorites.

6.2 Supernova νp-process

The hypernova is an extreme example of a νp-process nucleosynthesis site. Therefore, we extended the GCE model from Sasaki et al. (2022) [83] and include the contribution from the νp-process of supernova explosion [84]. The s-process GCE has been well analyzed and relatively valid compared with r-process or p-isotopes. Therefore we simply used the result from Kobayashi et al. (2020) [23] while other processes which take place in explosive astrophysical events are still unclear, there is a growing consensus that NSM is a r-process site. Before the formation of a neutron star binary, some single star explosion occurs. Such an explosive phenomena is also a source of heavy elements, such as r-process and νp-process. According to Kobayashi et al. 2020 [23], some fraction of single stars with $> 25M_{\odot}$ explode as hypernovae(HNe) whose explosion energy E_{exp} is higher than typical SNe by one order of magnitude, i.e., $E_{exp} \sim 10^{52}$ erg. Therefore, we assumed that the fraction of hypernova explosion increases linearly from 0 at $8M_{\odot}$ to 1 at $60M_{\odot}$ and stays 1 at $60M_{\odot} \leq M$.

Sasaki et al. (2021) showed that the explosion of massive stars such as Fujibayashi et al. 2015 [61] could explain the abundance of p-nuclei such as Mo, and that their effects could be observed as metal-poor element abundances.

Reichert et al. (2021) [84] suggested the νp-process occurs in rotating SNe. According to their models, νp-process and r-process occur in fast rotating SNe with strong magnetic fields(it may be a Hypernova) simultaneously. Not only the non-rotating supermassive star simulated by Fujibayashi et al. (2021) [85], this type of HNe should be considered. The Table 3 shows the combination of our νp-process GCE calculation.

6.2.1 The abundance pattern of p-nuclei

The calculated abundance of p-isotopes are shown in Figure 28. It is clearly shown that this model under produces ^{94}Mo and ^{96}Ru or overproduces ^{92}Mo. It is fairly reasonable since neutrino flux is relatively lower in explosions of a low mass progenitor model whereas SNe of supermassive stars produce a really high neutrino

Table 3. The model combination. Blank means no corresponding process occurs the sites. The full references are shown in text.

	s	γ	r	νp
SN Ia		Kusakabe		
NDW (light)		Travaglio	Reichert (OC-RRw)	
NDW (massive)		Travaglio	Fujibayashi	
MHDJ		Travaglio	Reichert (OC-Rs)	
AGB	Kobayashi	Kusakabe		

flux environment. The model in this study adopted only such extreme cases of SNe or HNe model for νp-process nucleosynthesis calculation. The intermediate mass progenitor model (30-80 $M_\odot$) will remarkably improve the fitness.

6.2.2 Isotopic ratio of each element

Figure 29-31 shows the isotopic ratio of Mo, Ru and Pd. In general, this study could reproduce a sufficient amount of total elemental abundances of Mo, Ru, Pd. However, some of their isotopes are overproduced and some are underproduced. Although it is obvious from the previous section of p-nuclei abundance, in this section, the detail of each element will be discussed including isotopes produced by r-process.

From ^{95}Mo to ^{100}Mo are well reproduced. However, ^{92}Mo is much abundant and ^{94}Mo is slightly insufficient. Again it is because this study does not adopt an intermediate mass SNe model which should produce a νp-process peak at A=94-96. Such nucleosynthesis calculation is awaited to reveal the νp-process production more precisely. In the Ru and Pd figures, a successful reproduction of the solar system composition can be seen. In this study, we considered the contribution from νp-process as a source of p-nuclei and also r-process as a source of neutron-rich isotopes simultaneously. As a result, the solar composition from neutron deficient side to neutron rich side is reasonably reproduced. This fact suggests that our assumption consisting our GCE calculation might be reasonable enough and not far from reality.

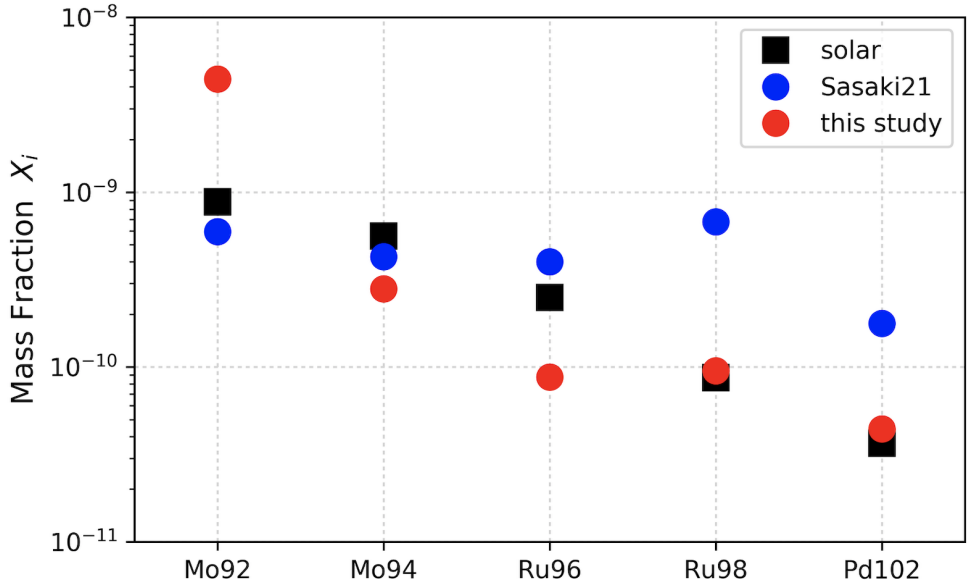

Fig. 28. The abundance of p-nuclei at the solar system metallicity in the version that considered SN νp-process contribution compared with Sasaki et al. 2022 [83].

6.2.3 The origin of each isotopes of Mo, Ru and Pd

Here, we shows an updated table of the origin of the three elements, Mo, Ru and Pd in Table 4. Many previous studies focus on the ratio between s-process and r-process. We, for the first time, separated the contribution from each astrophysical site. The s-process contribution comes from AGB stars. The single star in the table denotes the contribution from SNe and HNe; it may include the contribution from collapsar.

Large fractions of the five p-nuclei, ^{92}Mo, ^{94}Mo, ^{96}Ru, ^{98}Ru and ^{100}Pd, are created by νp-process, while small amounts are synthesized through γ-process as well. About 2% of ^{94}Mo is created by s-process. This is because that ^{93}Zr is a branching point of the s-process: The β-decay half life of ^{93}Zr is $\sim 1.61\times10^{6}$y [86]. This is comparable to the neutron capture time scale in the s-process. ^{93}Zr rarely β-decays to ^{93}Nb before they capture neutrons. This path creates a small fraction of ^{94}Mo by the s-process. The most neutron rich isotopes, ^{100}Mo, ^{104}Ru and ^{110}Pd are predominantly

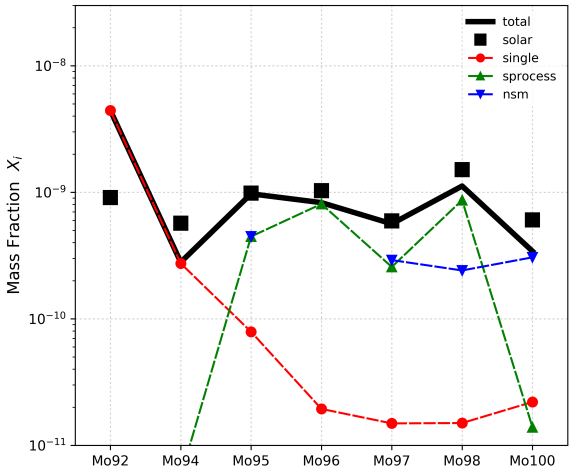

Fig. 29. The isotopic fractions of Mo at the solar metallicity. The red line shows the contribution from the collapsing single stars including CCSNe and hypernovae. The green and blue lines show the contribution from the s-process and NSM respectively. The black solid line show the sum of these three component.

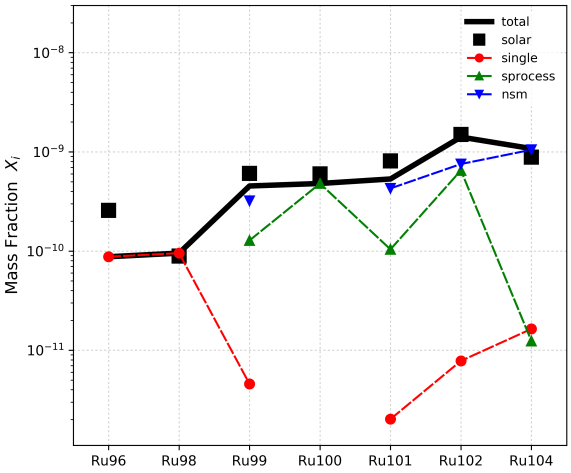

Fig. 30. The isotopic fractions of Ru at the solar metallicity.

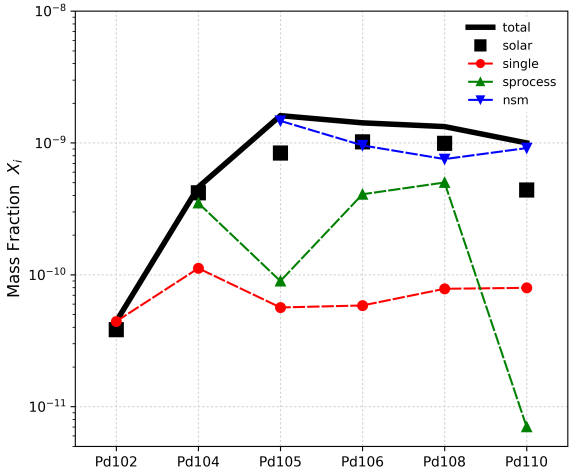

Fig. 31. The isotopic fractions of Pd at the solar metallicity.

Table 4. origin of isotopes (in %)

Element	Mass	s-process	nsm r-process	single star
Mo	92	0.0	0.0	100.0
	94	2.0	0.0	98.0
	95	46.0	45.9	8.1
	96	97.7	0.0	2.3
	97	45.7	51.7	2.6
	98	77.2	21.5	1.3
	100	4.1	89.5	6.4
Ru	96	0.0	0.0	100.0
	98	0.0	0.0	100.0
	99	28.1	70.8	1.0
	100	100.0	0.0	0.0
	101	19.5	80.1	0.4
	102	46.0	53.4	0.6
	104	1.1	97.3	1.5
Pd	102	0.0	0.0	100.0
	104	75.8	0.0	24.2
	105	5.5	91.0	3.5
	106	28.6	67.2	4.1
	108	37.6	56.6	5.9
	110	0.7	91.3	8.0

synthesized by the NSM r-process. These isotopes, produced only by the r-process, and the pure p-nuclei have even mass number.

In the context of GCE, the explosions of single massive stars CCSNe and collapsars, which are the astrophysical sites for the r-, νp- and γ-processes, occur from the very early phase of Galactic evolution. AGB stars, which are the major astrophysical sites for the s-process to produce heavier s-nuclei with A $\leq$ 90, follow later. The contribution from NSMs to the enrichment of heavy elements in the interstellar materials arises at much later epoch of cosmic evolution because of the long time delay of merging neutron stars.

These two facts that some specific processes predominantly synthesize isotopes having even mass numbers and that the contribution from each process exhibits different time delay in cosmic and Galactic evolution are the major sources to create

the time evolution of odd-even isotopic abundance ratios.

6.2.4 The evolution of odd-even ratio

The isotope separation by astronomical observation is still tough. However, some studies that separate the sum of odd isotopes and the sum of the even isotopes.

Mashokina et al. (2019) [87] determined the even-to-odd barium isotope ratio. Future astronomical observations with next-generation telescopes will provide us with isotope ratios for more elements. In advance of this kind of further observational development, we calculate the evolution of isotopic abundances of Mo, Ru and Pd and theoretically predict the isotopic ratio of these elements.

Figure 32 shows the evolution of Mo odd-even ratio as a function of metallicity. A clear decreasing feature at [Fe/H]>-2 can been seen. It is because that the earliest contributor is single star. Seeing Table 4, the single star component produces much $^{92,94}Mo$, which are even isotopes. Therefore, the odd-even ratio should have been significantly high in the metal poor era. Other components from s-process and NSM appear later, therefore the ratio decreases towards the present value at [Fe/H]=0. After the single massive star contribution, s-process follows because AGB stars have lighter masses and longer time delay due to longer lifetime of the main sequence phase. The s-process produces a half of the odd isotopes ^{95}Mo and ^{97}Mo. Therefore, the Mo isotope ratio decreases quickly from 1.7 downs to 0.9 around [Fe/H]≈-1. The last contributor is the NSM r-process. It produces the other half of ^{95}Mo and ^{97}Mo, then the isotope ratio decreases again before reaching the value of the solar system.

The similar feature can been seen in Ru case, too (Figure 33). Only 1% of ^{99}Ru is produced by the single star component. The s-process and NSM r-process contribution follow and the odd-even ratio decreases down to the present value. On the other hand, in the Pd case (Figure 34), the feature is not so clear. It is because the fraction of p-isotopes is very small in Pd in contrast to Mo and Ru. This is the clear difference between the elements which have high or low p-isotope fraction. Future observations can test this assumption and obtain the information on the origin of p-isotopes by using this scheme of identifying odd-even ratio of each element.

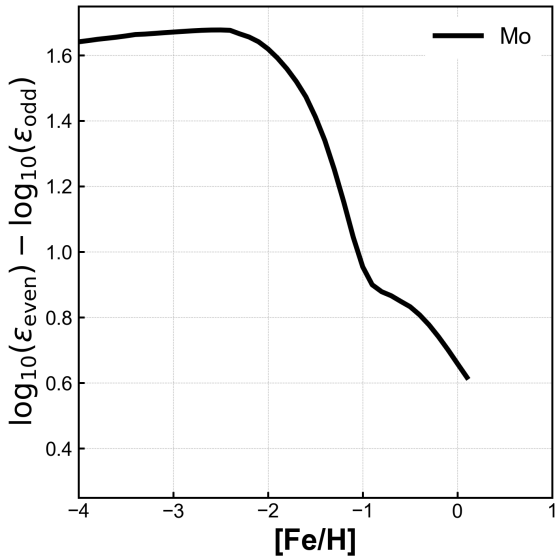

Fig. 32. The ratio between the odd and even isotopes of Mo as a function of metallicity in a logscale.

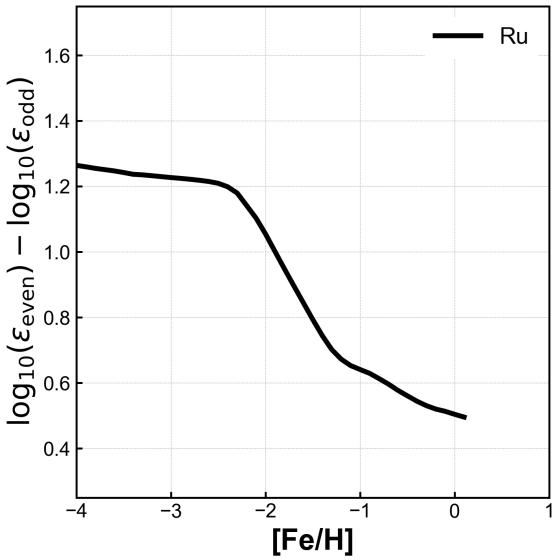

Fig. 33. The ratio between the odd and even isotopes of Ru as a function of metallicity in a logscale.

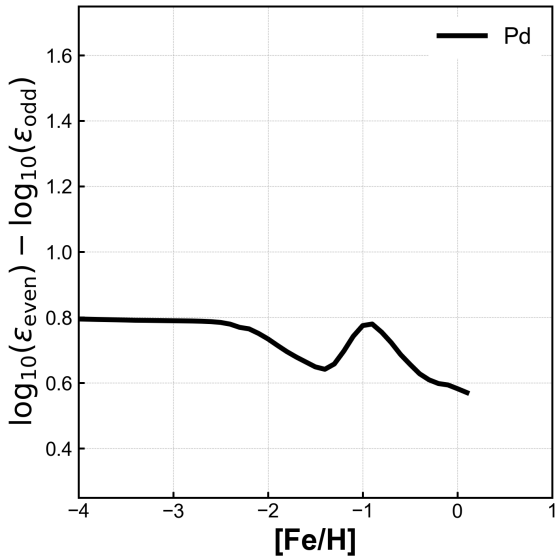

Fig. 34. The ratio between the odd and even isotopes of Pd as a function of metallicity in a logscale.

6.2.5 [X/Fe]-[Fe/H] plane

Figure 35 shows the evolutionary track of the [Mo/Fe] and [Ru/Fe] in the case that not only the HN νp-process but also SN νp-process are included. Basically, no visible difference is seen between the case with and without SN νp-process. In the previous two sections, we have discussed clear improvement of p-nuclei abundances and reasonable agreement with the measured solar system isotopic fractions of Mo, Ru and Pd by taking account of only the HN νp-process. SN νp-process has little impact on the elemental abundance of Mo and Ru.

There are two reasons for this fact: Firstly, although SN νp-process makes some differences in isotopic fractions, it does not have a large impact on the total elemental abundance of Mo or Ru. Therefore, the influence on [Mo/Fe] and [Ru/Fe] is limited and we still see almost the same trend in the [X/Fe]-[Fe/H] plane. Secondly, the very early Galaxy is dominated by supermassive stars, therefore, even in the case of including the contribution from SN νp-process, the feature at [Fe/H]<-2 is largely constrained by the collapsar νp-process.

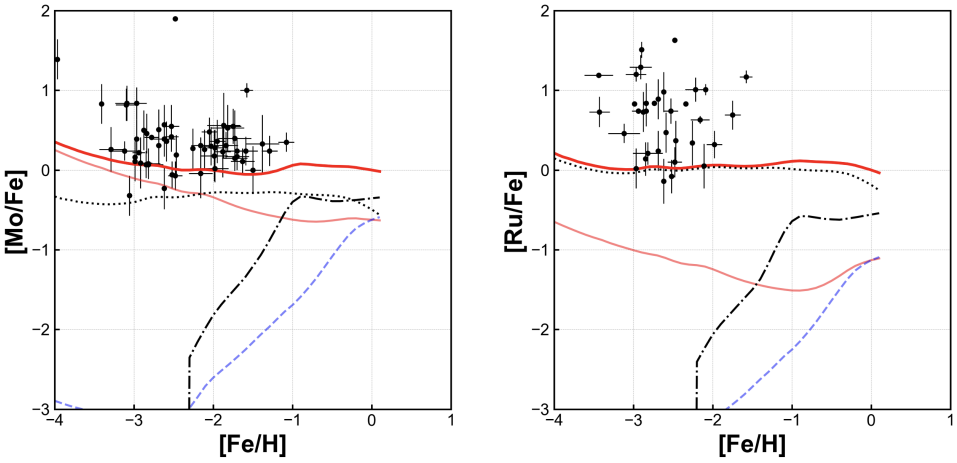

Fig. 35. Elemental abundance evolution of Mo and Ru. Thin lines show the same as Figure 26

In this study, we demonstrate the GCE of Mo and Ru by taking account of only two extreme contributions of the νp-process in collapsing single stars, i.e. HN with

very large mass and SN with relatively small mass. The nucleosynthesis data for SN νp-process are taken from Reichert et al. [84]. More sophisticated calculations including various contributions from intermediate mass models of SN νp-process is desirable to verify if our present crude study including only two extreme contributions is a good approximation. The extensive study is now underway.

6.3 Conclusion

The ^{92,94}Mo and ^{96,98}Ru contributions to the GCE of νp-processes in the neutrino-driven winds of core-collapse supernovae (including HNe in particular) are calculated. The contribution of the νp-process in normal SN II is negligible, but the contribution of the HN νp-process with heavy PNS is dominant. The contribution of the νp-process to the GCE of the νp-nuclei is dominant. The contribution of the HN νp-process to the GCE of the p-nucleus is largest at low metallicities.

The high [Mo/Fe] ratios observed in low-metallicity stars suggest that the HNe νp-process is a major source of ^{92,94}Mo and ^{96,98}Ru in the Galaxy.

In this study, we explored the possible effect of the νp-process on the GCE of ^{92,94}Mo and ^{96,98}Ru. It should be noted, however, that there are uncertainties in this analysis. First, the uncertainties due to the inverse shock effect and the fast flavor conversion of neutrinos are not taken into account. The potential effects of inverse shocks and neutrino fast flavor conversions were discussed in [65]. They may enhance the νp-process in SN II and have a non-negligible effect on the GCE of Mo and Ru, but these effects are still subject to large theoretical uncertainties. Long-term simulations of core-collapse supernovae beyond 1s are needed to more accurately include such uncertainties in the νp-process. A second caveat is that we estimate the p-nucleus yield based on one particular HN model, and the dependence of this result on primordial mass and metal abundance in the HN is not taken into account in the GCE calculation. This suggests that the GCE results for p-nuclei are not particularly sensitive to the HN primordial mass range. However, further study of the progenitor dependence of HN is needed to reach more quantitative conclusions.

We also tested the contribution from the νp-process by SNe. The possiblity to observe the contribution from νp-process still exist and the solar isotopic composition has been well reproduced. And, the odd-even ratio in the future observations will give us the important information of the origin of elements.

7 Summary and Conclusion of our GCE study for heavy elements

7.1 Summary

Many studies of r-process have been done both theoretically and observationally. Observed abundance pattern in individual stars was discussed by nucleosynthesis calculation with MHD simulations and statistical trend in [X/Fe] - [Fe/H] plane was evaluated by galactic chemical evolution studies. In this paper, we tried to reveal the evolution of abundance pattern in a GCE context. We take into account contribution from three astrophysical sites; CCSNe, NSM and collapsar. CCSNe have two types; NDW, producing only light r-process elements, and MHDJ, producing all r-process peaks. NSM has two ejecta. In a dynamical ejecta, electron fraction become very low and fissile nuclei can be produced, on the other hand, the condition in wind ejecta is similar to NDW and only the weak r-process occur. Although collapsar can produce all r-process peaks, the peak might be shifted to upper region due to extremely high value of entropy per baryon (Section 1.3).

Our model of the galactic gas evolution is based on Timmes *et al.* (1995). By extending their formula for Type Ia supernova, we formulate the galactic NSM rate taking account of binary coalescing time derived from GW energy loss rate. With this gas evolution calculation, we perform a GCE calculation and reveal the time evolution of r-process elements for each input of nucleosynthesis yields (Chapter 2, 3).

We find that CCSNe and collapsars are the dominant sources of r-process elements in the early Galaxy, while the NSM contributes to only a late phase of the galaxy

because of the cosmologically long timescale of orbital decay by GW radiation leading to a coalescence. This statement is independently valid from a minimum coalescence times τ_g, the combination of multiple r-process sites and the nuclear physics inputs.

The collapsars progenitor are more massive stars than supernovae therefore collapsars more likely occur in the very early galaxy and have dominant impact on the GCE. The variation of the relative contribution of each astrophysical site with galactic time results in the time-evolution of the r-process abundance pattern.

We find that significant differences among our multiple-site GCE model calculations arise in the isotopic abundance pattern as a function of mass number A, while still satisfying the universality of elemental abundances for metal-poor halo stars. This is in contrast to previous studies that focused on only a single r-process site or a combination of at most two astrophysical sites in order to explain the universality of the elemental abundance pattern.

Several unique features of each astrophysical site are still expected in the GCE of the isotopic mass A-abundance pattern. In particular, the collapsar contribution dominates from the very beginning of the early Galaxy since its progenitor is a very massive star. The collapsar r-process shows an odd-even pattern over the entire mass range. Also for both the collapsars and NSMs the abundance peaks shift towards the heavier mass region due to a high residual neutron-flux during the freezeout of the r-process.

Also, the origin of p-nuclei, which is on the proton-rich stable nuclei and typical fraction is less than 1.5%, is unclear. Mo and Ru have a large fraction of p-isotopes. γ-process produce some p-nuclei however the process underproduces Mo and Ru. Therefore, another process to create sufficient amount of p-isotopes of Mo and Ru observed in the solar system. Recent studies show νp-processes in HN and SN can produce large amount of p-nuclei. We, for the first time, include the HN νp-process and SN νp-process into a GCE calculation.

The νp-processes in HN and SN clearly enhance the final yields, abundance in the solar metallicity, of Mo and Ru in our GCE calculation. In both case, the Mo abundance in metal poor epoch is enhanced by $\sim$0.5 dex. By this enhancement, the

GCE result better match to the observed Mo abundance of galactic stars.

Our GCE calculation including s-process, r-process and νp-process simultaneously reasonably produce the fractions of all the isotopes of Mo, Ru and Pd. Moreover, we theoretically predict the evolution of odd-even ratio of Mo, Ru and Pd as a reference for future astronomical observations.

7.2 Conclusion

In this thesis, we make theoretical predictions about the origin and evolution of heavy elements, especially r-process elements and p-nuclei, from the perspective of GCE. In addition to this, we discussed their observability, and proposed future astronomical observations to be linked to a cross-cutting project between nuclear physics, astrophysics and astronomy. Here we summarize our conclusions.

1. We revealed that the isotopic abundance pattern of r-process elements have changed over the galactic history without violating the r-process universality. We obtained a theoretical prediction of a 'template' of r-process abundance pattern at every metallicity, a measure of time, from the birth of galaxy (Section 4.1.2). We can see the time variation in the r-process abundance patterns, however the universality in elemental abundance pattern is still satisfied (Section 4.1.3). This will be a great measure of future observations. Moreover, we demonstrate the possibilities to prove the contribution of collapsar by analyse the zig-zag pattern that collapsar produce. This can be observed in the isotopic ratio or just elemental abundance of Eu and Sm.

2. We demonstrated the νp-process in the supernovae and hypernovae can produce a sufficient amount of the p-nuclei in the solar system for the first time (Section 6, 6.2). Even in elemental abundance, Mo abundance is considerably enhanced by νp-process by around 0.5 dex and astronomical observations favor this trend (Section 6.1.2). Also the odd-even ratio of Mo and Ru has changed dramatically through the galactic history. The odd-even ratio is enough observable and future next-generation telescopes will provide us with the 'evidence' of νp-process nucleosynthesis in supernova and hypernova.

Thus, we provide the theoretical prediction of the time evolution of r-process elements and p-nuclei with great importance to reveal the origin of heavy elements in the universe.

References

[1] Christopher Sneden, John J Cowan, and Roberto Gallino. Neutron-capture elements in the early galaxy. *Annu. Rev. Astron. Astrophys.*, 46:241–288, 2008.

[2] Satoshi Honda, W Aoki, Y Ishimaru, S Wanajo, and SG Ryan. Neutron-capture elements in the very metal poor star hd 122563. *The Astrophysical Journal*, 643(2):1180, 2006.

[3] Satoshi Honda, Wako Aoki, Yuhri Ishimaru, and Shinya Wanajo. Neutron-capture elements in the very metal-poor star hd 88609: another star with excesses of light neutron-capture elements. *The Astrophysical Journal*, 666(2):1189, 2007.

[4] Misa Aoki, Yuhri Ishimaru, Wako Aoki, and Shinya Wanajo. Diversity of abundance patterns of light neutron-capture elements in very-metal-poor stars2217. *The Astrophysical Journal*, 837(1):8, 2017.

[5] S Shibagaki, T Kajino, GJ Mathews, S Chiba, S Nishimura, and G Lorusso. Relative contributions of the weak, main, and fission-recycling r-process. *The Astrophysical Journal*, 816(2):79, 2016.

[6] Shinya Wanajo. The r-process in proto-neutron-star wind revisited. *The Astrophysical Journal Letters*, 770(2):L22, 2013.

[7] Christian Winteler, Roger Kaeppeli, Albino Perego, Almudena Arcones, Nicolas Vasset, Nobuya Nishimura, Matthias Liebendoerfer, and F-K Thielemann. Magnetorotationally driven supernovae as the origin of early galaxy r-process elements? *The astrophysical journal letters*, 750(1):L22, 2012.

[8] Nobuya Nishimura, Toshitaka Kajino, Grant J Mathews, Shunji Nishimura, and Toshio Suzuki. Impact of new β-decay half-lives on r-process nucleosynthesis. *Physical Review C*, 85(4):048801, 2012.

[9] Dirk Martin, Albino Perego, Almudena Arcones, Oleg Korobkin, and Friedrich-Karl Thielemann. Nucleosynthesis in the ejecta of neutron star mergers. *arXiv preprint arXiv:1509.07628*, 2015.

[10] Toshio Suzuki, Shota Shibagaki, Takashi Yoshida, Toshitaka Kajino, and Takaharu Otsuka. β-decay rates for exotic nuclei and r-process nucleosynthesis up to thorium and uranium. *The Astrophysical Journal*, 859(2):133, 2018.

[11] Ko Nakamura, Toshitaka Kajino, GJ Mathews, S Sato, and S Harikae. r-process nucleosynthesis in the mhd+ neutrino-heated collapsar jet. *Astronomy & Astrophysics*, 582:A34, 2015.

[12] Paolo A Mazzali, Jinsong Deng, Elena Pian, Daniele Malesani, Nozomu Tominaga, Keiichi Maeda, Ken'ichi Nomoto, Guido Chincarini, Stefano Covino, Massimo Della Valle, et al. Models for the type ic hypernova sn 2003lw associated with grb 031203. *The Astrophysical Journal*, 645(2):1323, 2006.

[13] Daniel M Siegel, Jennifer Barnes, and Brian D Metzger. Collapsars as a major source of r-process elements. *Nature*, 569(7755):241–244, 2019.

[14] D Argast, Ma Samland, F-K Thielemann, and Y-Z Qian. Neutron star mergers versus core-collapse supernovae as dominant r-process sites in the early galaxy. *Astronomy & Astrophysics*, 416(3):997–1011, 2004.

[15] Yutaka Hirai, Yuhri Ishimaru, Takayuki R Saitoh, Michiko S Fujii, Jun Hidaka, and Toshitaka Kajino. Enrichment of r-process elements in dwarf spheroidal galaxies in chemo-dynamical evolution model. *The Astrophysical Journal*, 814(1):41, 2015.

[16] Paz Beniamini and Tsvi Piran. The gravitational waves merger time distribution of binary neutron star systems. *Monthly Notices of the Royal Astronomical Society*, 487(4):4847–4854, 2019.

[17] Tomonori Totani, Tomoki Morokuma, Takeshi Oda, Mamoru Doi, and Naoki Yasuda. Delay Time Distribution Measurement of Type Ia Supernovae by the Subaru/XMM-Newton Deep Survey and Implications for the Progenitor. *Publications of the Astronomical Society of Japan*, 60(6):1327–1346, 12 2008.

[18] Paolo Simonetti, Francesca Matteucci, Laura Greggio, and Gabriele Cescutti. A new delay time distribution for merging neutron stars tested against galactic and cosmic data. *Monthly Notices of the Royal Astronomical Society*, 486(2):2896–2909, 2019.

[19] FX Timmes, SE Woosley, and Thomas A Weaver. Galactic chemical evolution: Hydrogen through zinc. *The Astrophysical Journal Supplement Series*, 98:617–658, 1995.

[20] SE Woosley and Thomas A Weaver. The evolution and explosion of massive stars ii: Explosive hydrodynamics and nucleosynthesis. Technical report, Lawrence Livermore National Lab., CA (United States), 1995.

[21] G Schaller, D Schaerer, G Meynet, and A Maeder. New grids of stellar models from 0.8 to 120 solar masses at z= 0.020 and z= 0.001. *Astronomy and Astrophysics Supplement Series*, 96:269–331, 1992.

[22] Pavel Kroupa. On the variation of the initial mass function. *Monthly Notices of the Royal Astronomical Society*, 322(2):231–246, 2001.

[23] Chiaki Kobayashi, Amanda I Karakas, and Maria Lugaro. The origin of elements from carbon to uranium. *The Astrophysical Journal*, 900(2):179, 2020.

[24] Benoit Côté, Chris L Fryer, Krzysztof Belczynski, Oleg Korobkin, Martyna Chruślińska, Nicole Vassh, Matthew R Mumpower, Jonas Lippuner, Trevor M Sprouse, Rebecca Surman, et al. The origin of r-process elements in the milky way. *The Astrophysical Journal*, 855(2):99, 2018.

[25] Michael Famiano, A Baha Balantekin, Toshitaka Kajino, Motohiko Kusakabe, Kanji Mori, and Yudong Luo. Nuclear reaction screening, weak interactions, and r-process nucleosynthesis in high magnetic fields. *The Astrophysical Journal*, 898(2):163, 2020.

[26] Darach Watson, Camilla J Hansen, Jonatan Selsing, Andreas Koch, Daniele B Malesani, Anja C Andersen, Johan PU Fynbo, Almudena Arcones, Andreas Bauswein, Stefano Covino, et al. Identification of strontium in the merger of two neutron stars. *Nature*, 574(7779):497–500, 2019.

[27] Kenta Hotokezaka, Paz Beniamini, and Tsvi Piran. Neutron star mergers as sites of r-process nucleosynthesis and short gamma-ray bursts. *International Journal of Modern Physics D*, 27(13):1842005, 2018.

[28] T. Kajino, W. Aoki, A.B. Balantekin, R. Diehl, M.A. Famiano, and G.J. Mathews. Current status of r-process nucleosynthesis. *Progress in Particle and Nuclear Physics*, 107:109 – 166, 2019.

[29] AI MacFadyen and SE Woosley. Collapsars: Gamma-ray bursts and explosions in "failed supernovae". *The Astrophysical Journal*, 524(1):262, 1999.

[30] Rebecca Surman, GC McLaughlin, and WR Hix. Nucleosynthesis in the outflow from gamma-ray burst accretion disks. *The Astrophysical Journal*, 643(2):1057, 2006.

[31] Seiji Harikae, Tomoya Takiwaki, and Kei Kotake. Long-term evolution of slowly rotating collapsar in special relativistic magnetohydrodynamics. *The Astrophysical Journal*, 704(1):354, 2009.

[32] Tomoya Takiwaki, Kei Kotake, and Katsuhiko Sato. Special relativistic simulations of magnetically dominated jets in collapsing massive stars. *The Astrophysical Journal*, 691(2):1360, 2009.

[33] Oleg Korobkin, Aimee M Hungerford, Christopher L Fryer, Matthew R Mumpower, G Wendell Misch, Trevor M Sprouse, Jonas Lippuner, Rebecca Surman, Aaron J Couture, Peter F Bloser, et al. Gamma rays from kilonova: a potential probe of r-process nucleosynthesis. *The Astrophysical Journal*, 889(2):168, 2020.

[34] O Korobkin, Stephan Rosswog, A Arcones, and C Winteler. On the astrophysical robustness of the neutron star merger r-process. *Monthly Notices of the Royal Astronomical Society*, 426(3):1940–1949, 2012.

[35] Tsvi Piran, Ehud Nakar, and Stephan Rosswog. The electromagnetic signals of compact binary mergers. *Monthly Notices of the Royal Astronomical Society*, 430(3):2121–2136, 2013.

[36] Stephan Rosswog, T Piran, and E Nakar. The multimessenger picture of compact object encounters: binary mergers versus dynamical collisions. *Monthly Notices of the Royal Astronomical Society*, 430(4):2585–2604, 2013.

[37] Stephan Rosswog and Matthias Liebendoerfer. High-resolution calculations of merging neutron stars—ii. neutrino emission. *Monthly Notices of the Royal Astronomical Society*, 342(3):673–689, 2003.

[38] F-K Thielemann, M Eichler, IV Panov, and B Wehmeyer. Neutron star mergers and nucleosynthesis of heavy elements. *Annual Review of Nuclear and Particle Science*, 67:253–274, 2017.

[39] Yuta Yamazaki, Zhenyu He, Toshitaka Kajino, Grant J Mathews, Michael A Famiano, Xiaodong Tang, and Jianrong Shi. Possibility to identify the contributions from collapsars, supernovae, and neutron star mergers from the evolution of the r-process mass abundance distribution. *The Astrophysical Journal*, 933(1):112, 2022.

[40] Ian U Roederer, James E Lawler, Jennifer S Sobeck, Timothy C Beers, John J Cowan, Anna Frebel, Inese I Ivans, Hendrik Schatz, Christopher Sneden, and

Ian B Thompson. New hubble space telescope observations of heavy elements in four metal-poor stars. *The Astrophysical Journal Supplement Series*, 203(2):27, 2012.

[41] Christopher Sneden, John J Cowan, James E Lawler, Inese I Ivans, Scott Burles, Timothy C Beers, Francesca Primas, Vanessa Hill, James W Truran, George M Fuller, et al. The extremely metal-poor, neutron capture-rich star cs 22892-052: a comprehensive abundance analysis. *The Astrophysical Journal*, 591(2):936, 2003.

[42] L Mashonkina, N Christlieb, and Kjell Eriksson. The hamburg/eso r-process enhanced star survey (heres)-x. he 2252- 4225, one more r-process enhanced and actinide-boost halo star. *Astronomy & Astrophysics*, 569:A43, 2014.

[43] E. Margaret Burbidge, G. R. Burbidge, William A. Fowler, and F. Hoyle. Synthesis of the Elements in Stars. *Reviews of Modern Physics*, 29(4):547–650, January 1957.

[44] S. E. Woosley and W. M. Howard. The p-processes in supernovae. *The Astrophysical Journal Supplement Series*, 36:285–304, February 1978.

[45] T. Hayakawa, N. Iwamoto, T. Shizuma, T. Kajino, H. Umeda, and K. Nomoto. Evidence for nucleosynthesis in the supernova γ process: Universal scaling for p nuclei. *Physical Review Letters*, 93:161102, Oct 2004.

[46] M. Rayet, M. Arnould, and N. Prantzos. The p-process revisited. *Astronomy and Astrophysics*, 227(1):271–281, January 1990.

[47] N. Prantzos, M. Hashimoto, M. Rayet, and M. Arnould. The p-process in SN 1987A. *Astronomy and Astrophysics*, 238:455–461, November 1990.

[48] M. Rayet, M. Arnould, M. Hashimoto, N. Prantzos, and K. Nomoto. The p-process in Type II supernovae. *Astronomy and Astrophysics*, 298:517, June 1995.

[49] Takehito Hayakawa, Nobuyuki Iwamoto, Toshitaka Kajino, Toshiyuki Shizuma, Hideyuki Umeda, and Ken'ichi Nomoto. Empirical Abundance Scaling Laws and Implications for the Gamma Process in Core-Collapse Supernovae. *The Astrophysical Journal*, 685(2):1089–1102, October 2008.

[50] W. Michael Howard, Bradley S. Meyer, and S. E. Woosley. A New Site for the Astrophysical Gamma-Process. *The Astrophysical Journal Letters*, 373:L5, May 1991.

[51] S. Goriely, J. José, M. Hernanz, M. Rayet, and M. Arnould. He-detonation in sub-Chandrasekhar CO white dwarfs: A new insight into energetics and p-process nucleosynthesis. *Astronomy and Astrophysics*, 383:L27–L30, March 2002.

[52] Motohiko Kusakabe, Nobuyuki Iwamoto, and Ken'ichi Nomoto. Production of the p-process Nuclei in the Carbon-deflagration Model for Type Ia Supernovae. *The Astrophysical Journal*, 726(1):25, January 2011.

[53] C. Travaglio, F. K. Röpke, R. Gallino, and W. Hillebrandt. Type Ia Supernovae as Sites of the p-process: Two-dimensional Models Coupled to Nucleosynthesis. *The Astrophysical Journal*, 739(2):93, October 2011.

[54] C. Travaglio, R. Gallino, T. Rauscher, F. K. Röpke, and W. Hillebrandt. Testing the Role of SNe Ia for Galactic Chemical Evolution of p-nuclei with Two-dimensional Models and with s-process Seeds at Different Metallicities. *The Astrophysical Journal*, 799(1):54, January 2015.

[55] C. Travaglio, T. Rauscher, A. Heger, M. Pignatari, and C. West. Role of Core-collapse Supernovae in Explaining Solar System Abundances of p Nuclides. *The Astrophysical Journal*, 854(1):18, February 2018.

[56] C. Fröhlich, G. Martínez-Pinedo, M. Liebendörfer, F. K. Thielemann, E. Bravo, W. R. Hix, K. Langanke, and N. T. Zinner. Neutrino-Induced Nucleosynthesis of A¿64 Nuclei: The νp Process. *Physical Review Letters*, 96(14):142502, April 2006.

[57] J. Pruet, R. D. Hoffman, S. E. Woosley, H. T. Janka, and R. Buras. Nucleosynthesis in Early Supernova Winds. II. The Role of Neutrinos. *The Astrophysical Journal*, 644(2):1028–1039, June 2006.

[58] Shinya Wanajo. The rp-Process in Neutrino-driven Winds. *The Astrophysical Journal*, 647(2):1323–1340, August 2006.

[59] Shinya Wanajo, Hans-Thomas Janka, and Shigeru Kubono. Uncertainties in the νp-process: Supernova Dynamics Versus Nuclear Physics. *The Astrophysical Journal*, 729(1):46, March 2011.

[60] A. Arcones, C. Fröhlich, and G. Martínez-Pinedo. Impact of Supernova Dynamics on the νp-process. *The Astrophysical Journal*, 750(1):18, May 2012.

[61] Sho Fujibayashi, Takashi Yoshida, and Yuichiro Sekiguchi. Nucleosynthesis in Neutrino-driven Winds in Hypernovae. *The Astrophysical Journal*, 810(2):115, September 2015.

[62] H. Sasaki, T. Kajino, T. Takiwaki, T. Hayakawa, A. B. Balantekin, and Y. Pehlivan. Possible effects of collective neutrino oscillations in three-flavor multiangle simulations of supernova ν p processes. *Physical Review D.*, 96(4):043013, August 2017.

[63] J. Bliss, A. Arcones, and Y. Z. Qian. Production of Mo and Ru Isotopes in Neutrino-driven Winds: Implications for Solar Abundances and Presolar Grains. *The Astrophysical Journal*, 866(2):105, October 2018.

[64] N. Nishimura, T. Rauscher, R. Hirschi, G. Cescutti, A. St J. Murphy, and C. Fröhlich. Uncertainties in νp-process nucleosynthesis from Monte Carlo variation of reaction rates. *MNRAS*, 489(1):1379–1396, October 2019.

[65] Zewei Xiong, Andre Sieverding, Manibrata Sen, and Yong-Zhong Qian. Potential Impact of Fast Flavor Oscillations on Neutrino-driven Winds and Their Nucleosynthesis. *The Astrophysical Journal*, 900(2):144, September 2020.

[66] Shilun Jin, Luke F. Roberts, Sam M. Austin, and Hendrik Schatz. Enhanced triple-α reaction reduces proton-rich nucleosynthesis in supernovae. *Nature*, 588(7836):57–60, January 2020.

[67] Toshiki Sato, Keiichi Maeda, Shigehiro Nagataki, Takashi Yoshida, Brian Grefenstette, Brian J. Williams, Hideyuki Umeda, Masaomi Ono, and John P. Hughes. High-entropy ejecta plumes in Cassiopeia A from neutrino-driven convection. *Nature*, 592(7855):537–540, January 2021.

[68] N. Dauphas, B. Marty, and L. Reisberg. Molybdenum evidence for inherited planetary scale isotope heterogeneity of the protosolar nebula. *The Astrophysical Journal*, 565(1):640–644, jan 2002.

[69] Gerrit Budde, Christoph Burkhardt, Gregory A. Brennecka, Mario Fischer-G00F6dde, Thomas S. Kruijer, and Thorsten Kleine. Molybdenum isotopic evidence for the origin of chondrules and a distinct genetic heritage of carbonaceous and non-carbonaceous meteorites. *Earth and Planetary Science Letters*, 454:293–303, 2016.

[70] Graeme M. Poole, Mark Rehk00E4mper, Barry J. Coles, Tatiana Goldberg, and Caroline L. Smith. Nucleosynthetic molybdenum isotope anomalies in iron meteorites - new evidence for thermal processing of solar nebula material. *Earth and Planetary Science Letters*, 473:215–226, 2017.

[71] Fiorenzo Vincenzo, Todd A. Thompson, David H. Weinberg, Emily J. Griffith, James W. Johnson, and Jennifer A. Johnson. Nucleosynthesis signatures of neutrino-driven winds from proto-neutron stars: a perspective from chemical evolution models. *arXiv e-prints*, page arXiv:2102.04920, February 2021.

[72] Shinya Wanajo, Bernhard Müller, Hans-Thomas Janka, and Alexander Heger. Nucleosynthesis in the Innermost Ejecta of Neutrino-driven Supernova Explosions in Two Dimensions. *The Astrophysical Journal*, 852(1):40, January 2018.

[73] Kaori Otsuki, Hideyuki Tagoshi, Toshitaka Kajino, and Shin-ya Wanajo. General Relativistic Effects on Neutrino-driven Winds from Young, Hot Neutron Stars and r-Process Nucleosynthesis. *The Astrophysical Journal*, 533(1):424–439, April 2000.

[74] Adam Burrows, David Radice, David Vartanyan, Hiroki Nagakura, M. Aaron Skinner, and Joshua C. Dolence. The overarching framework of core-collapse supernova explosions as revealed by 3D FORNAX simulations. *MNRAS*, 491(2):2715–2735, January 2020.

[75] Hiroki Nagakura, Adam Burrows, David Vartanyan, and David Radice. Core-collapse supernova neutrino emission and detection informed by state-of-the-art three-dimensional numerical models. *MNRAS*, 500(1):696–717, January 2021.

[76] S. E. Woosley, D. H. Hartmann, R. D. Hoffman, and W. C. Haxton. The nu -Process. *The Astrophysical Journal*, 356:272, June 1990.

[77] Richard B Larson. A model for the formation of a spherical galaxy. *Monthly Notices of the Royal Astronomical Society*, 145(4):405–422, 1969.

[78] Isaac Shivvers, Maryam Modjaz, WeiKang Zheng, Yuqian Liu, Alexei V Filippenko, Jeffrey M Silverman, Thomas Matheson, Andrea Pastorello, Or Graur, Ryan J Foley, et al. Revisiting the lick observatory supernova search volume-limited sample: Updated classifications and revised stripped-envelope supernova fractions. *Publications of the Astronomical Society of the Pacific*, 129(975):054201, 2017.

[79] Takuma Suda, Yutaka Katsuta, Shimako Yamada, Tamon Suwa, Chikako Ishizuka, Yutaka Komiya, Kazuo Sorai, Masayuki Aikawa, and Masayuki Y Fujimoto. Stellar abundances for the galactic archeology (saga) database—compilation of the characteristics of known extremely metal-poor stars. *Publications of the Astronomical Society of Japan*, 60(5):1159–1171, 2008.

[80] S. Bisterzo, C. Travaglio, R. Gallino, M. Wiescher, and F. Käppeler. Galactic Chemical Evolution and Solar s-process Abundances: Dependence on the ^{13}C-pocket Structure. *The Astrophysical Journal*, 787(1):10, May 2014.

[81] Yuhri Ishimaru and Shinya Wanajo. Enrichment of the R-Process Element Europium in the Galactic Halo. *The Astrophysical Journal Letters*, 511(1):L33–L36, January 1999.

[82] Shinya Wanajo and Yuhri Ishimaru. r-process calculations and Galactic chemical evolution. *Nuclear Physics A*, 777:676–699, October 2006.

[83] Hirokazu Sasaki, Yuta Yamazaki, Toshitaka Kajino, Motohiko Kusakabe, Takehito Hayakawa, Myung-Ki Cheoun, Heamin Ko, and Grant J. Mathews. Impact of Hypernova νp-process Nucleosynthesis on the Galactic Chemical Evolution of Mo and Ru. *The Astrophysical Journal*, 924(1):29, January 2022.

[84] Moritz Reichert, Martin Obergaulinger, Marius Eichler, M Á Aloy, and Almudena Arcones. Nucleosynthesis in magneto-rotational supernovae. *Monthly Notices of the Royal Astronomical Society*, 501(4):5733–5745, 2021.

[85] Sho Fujibayashi, Koh Takahashi, Yuichiro Sekiguchi, and Masaru Shibata. Ultra-delayed neutrino-driven explosion of rotating massive-star collapse. *arXiv e-prints*, page arXiv:2102.04467, February 2021.

[86] Jinling Yang, Shengdong Zhang, Youqian Ding, Fujun Shu, and Jilong Zhang. A new value of 93zr half-life. *rca-Radiochimica Acta*, 98(2):59–63, 2010.

[87] LI Mashonkina and Andrey K Belyaev. Even-to-odd barium isotope ratio in selected galactic halo stars. *Astronomy Letters*, 45:341–352, 2019.